6-14-2012

Calibration of a Silver Detector using a PuBe Source

Melanie E. Mace

Follow this and additional works at: https://scholar.afit.edu/etd

Part of the Nuclear Commons

CALIBRATION OF A SILVER DETECTOR USING A PUBE SOURCE

THESIS

Melanie E. Mace, Captain, USAF

AFIT/NUCL/ENP/12-J01

DEPARTMENT OF THE AIR FORCE
AIR UNIVERSITY

AIR FORCE INSTITUTE OF TECHNOLOGY

Wright-Patterson Air Force Base, Ohio

The views expressed in this document are those of the author and do not reflect the official policy or position of the United States Air Force, the United States Department of Defense or the United States Government. This material is declared a work of the U.S. Government and is not subject to copyright protection in the United States.

AFIT/NUCL/ENP/12-J01

CALIBRATION OF A SILVER DETECTOR USING A PUBE SOURCE

THESIS

Presented to the Faculty

Department of Engineering Physics

Graduate School of Engineering and Management

Air Force Institute of Technology

Air University

Air Education and Training Command

in Partial Fulfillment of the Requirements for the

Degree of Master of Science in Nuclear Engineering

Melanie E. Mace, BS

Captain, USAF

June 2012

DISTRIBUTION STATEMENT A

APPROVED FOR PUBLIC RELEASE; DISTRIBUTION UNLIMITED.

AFIT/NUCL/ENP/12-J01

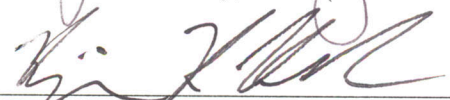CALIBRATION OF A SILVER DETECTOR USING A PUBE SOURCE
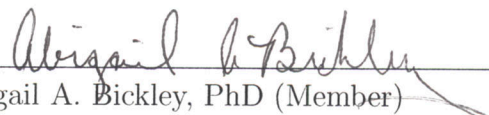
Melanie E. Mace, BS
Captain, USAF

Approved:

_____
John W. McClory, PhD (Chairman)

7 JUN 2012
_____
Date

_____
Maj Benjamin R. Kowash (Member)

7 Juh 2012
_____
Date

_____
Abigail A. Bickley, PhD (Member)

7 Jun 2012
_____
Date

Abstract

During the initial design of the Field Reversed Compression and Heating Experiment (FRCHX), magnetohydrodynamic simulations performed by Los Alamos National Laboratory using MACH2 predicted a neutron yield on the order of 10^{12} neutrons. However, Air Force Research Laboratory (AFRL) measurements indicate a total of 10^7-10^8 neutrons are generated from the FRCHX. The disagreement between the experimental and simulated neutron yield implies the simulation, the neutron detection system, and/or the FRCHX device need to be better understood. The objective of this thesis was to characterize the neutron detection system used at the FRCHX to determine the nominal calibration factors. The type of silver detector used in the FRCHX experiment consists of four silver foil wrapped Geiger-Müller tubes enclosed in a single block of polyethylene. To replicate the FRCHX set up, a PuBe source was used to create a burst of neutrons to calibrate an AFRL silver detector based on distance. It was determined that the calibration equation in use by AFRL for the silver detectors was correct within error at most distances. An alternate calibration equation was determined to be $F_{PuBe} = 12.2D^2 + 3020D$ where D is the distance in inches from the source to the front face of the silver detector. This equation was found using least squares techniques to reduce the residuals of the data collected using the PuBe source. The new calibration of AFRL's silver detectors does not account for the large order of magnitude difference observed between experiment and simulation. More research will be necessary to fully understand the discrepancy.

Acknowledgements

I would like to give thanks to my advisor for his guidance and patience. To my committee members who provided a wealth of knowledge and support. To Greg, Steve, and Joel, my fellow classmates, and Mr. Taylor who helped set up and/or troubleshoot my experiment. To Tony for collaborating on classwork in a fun yet productive way. To my parents for supporting me through all of my education goals. To my husband for loving and supporting me through this and all endeavors. Finally, I would like to thank my son for being the healthy, adventurous, curious boy that he is suppose to be.

Melanie E. Mace

Table of Contents

List of Figures

Figure   Page

ix

Figure Page

List of Tables

List of Abbreviations

CALIBRATION OF A SILVER DETECTOR USING A PUBE SOURCE

I. Introduction

There are various ways of harnessing energy to produce electricity necessary for our way of life. Coal, natural gas, wind, water, the sun and the atom are some examples of sources from which energy can be extracted. Fission is the current method used to extract energy from atomic nuclei. When nuclei fission they split producing fission fragments and energy that is released predominantly in the form of heat. This heat is used to produce steam driving a steam turbine to produce electricity. The isotopes that are fissile are radioactive and produce radioactive byproducts. The used fuel maintains the radioactive byproducts and therefore must be stored until the radiation levels are no longer harmful.

The sun is powered by a different nuclear process called fusion in which light nuclei combine to form more stable heavier nuclei and release energy. Sustainable fusion, if mastered, would provide a relatively cheap and clean energy alternative. The lightest nucleus is hydrogen which is abundant in nature, meaning the fuel for fusion would be almost limitless. The byproducts of fusion depend on the reaction. Many fusion reactions produce neutrons, protons and/or alphas along with other isotopes. The isotopes are usually stable, therefore radioactive waste is minimized to materials that are activated by neutron output, shown in Section 2.1. However, the temperatures and densities required to fuse nuclei are extreme and the ability to control fusion is still being perfected.

The Air Force Research Laboratory (AFRL) has been researching Magnetized Target Fusion (MTF) powered by the Shiva Star capacitors at Kirtland Air Force Base,

1

NM. The plasma performance is principally diagnosed using accurate, absolutely calibrated measurements of the neutron source strength and yield [5, 12]. Therefore, neutrons are measured to quantify the success of the fusion. Various neutron detectors including silver detectors, bubble detectors, and neutron TLDs are used. It has been necessary to place diagnostic detectors far from the MTF device to prevent detector damage and the loss of information. The silver detectors are fixed 48" away from the fusion device in the same horizontal plane as the explosion. The bubble detectors and neutron TLDs are place randomly around the MTF device.

During the initial design of the MTF device, magnetohydrodynamic (MHD) simulations performed by Los Alamos National Laboratory (LANL) using MACH2 predicted a neutron yield on the order of 10^{12} neutrons [26]. However, AFRL measurements indicate a total of 10^7-10^8 neutrons are generated from the MTF. The disagreement between the experimental and simulated neutron yield implies the simulation, the neutron detection system, and/or the MTF device need to be better understood. The goal of this research will be to create confidence in the neutron detection system by examining the silver detectors to ensure proper calibration.

Using various types of neutron detection devices are necessary to gain relevant comparative information regarding a neutron production system. Absolute calibrations can be accomplished using in situ neutron sources such as ^{252}Cf point sources and Deuterium-Deuterium (D-D) or Deuterium-Tritium (D-T) neutron generators [5]. For measurement of intensive or burst-like neutron emissions, a detector that utilizes neutron activation is a more appropriate detector than those that use gas or solid state mechanisms [12]. If the source used for calibration has a known neutron flux, the detector efficiency can be determine by allowing a neutron activated detector to reach saturation [12]. The silver detector used by AFRL uses neutron activation

2

to count signals. Those signals must be calibrated to a known source to have any meaning, which was accomplished by this research.

The silver detectors used at AFRL were designed based on the schematics described in the 1966 Lanter and Bannerman paper titled "The Silver Counter: A Detector for Bursts of Neutrons" [16]. These detectors use Geiger-Müller (G-M) tubes to count the silver decays from the neutron activation of a silver foil. The silver detectors were designed to determine the neutron yield of a burst of neutrons created by a single pulse from a neutron source using a calibration curve. The detectors do not count signals from the G-M tubes until after the end of the burst of neutrons. This allows time for the gammas from the burst of neutrons, neutron captures and scattered neutrons to leave the area. Thus, they are not counted during the measurement. The use of silver allows for a quick determination of the neutron yield after the end of the burst due to the short half-lives of the silver isotopes. AFRL calibrated the silver detectors with a single pulse from a neutron generator that had an unknown neutron yield, therefore, the calibration is uncertain and a new calibration of the detector will be accomplished.

Shots at Shiva Star were not possible due to funding and the use of a similar fusion neutron generator was not possible due to availability. Therefore, a PuBe source was used to calibrate the silver detector. One silver detector, along with six G-M tubes were sent to the Air Force Institute of Technology (AFIT) to be tested. The individual G-M tubes were examined using known beta and gamma sources. Ideal operational voltage, dead-time determination, and efficiency measurements were accomplished on each G-M tube. The silver detector was measured at distances ranging from 2.25" to 60" away from a 4.6 Ci PuBe source. The PuBe source was manually exposed and lowered. Counts from the detector after the source was lowered were measured using

3

counting electronics. The data was analyzed and a calibration curve was created and compared with existing calibration curves for this type of silver detector.

THESIS GOALS

- Characterize the Geiger-Müller tubes used in AFRL's silver detector.

- Determine silver foil activity based on signals measured by the silver detector due to bursts of neutrons at various distances.

- Create a calibration curve (useful in determining unknown neutron yields of sources) based on counts measured by the silver detector and compare the curve to previously published calibration curves from detectors of the same design.

This research shows that the AFRL silver detectors were properly calibrated at the distance of interest, but the calibration curve was incorrect. However, the difference in calibration was not significant enough to affect the four order magnitude difference between simulation and experiment. A calibration curve was created and compared to the calibration curve created by Lanter and Bannerman [16], as well as the calibration curve that was in use by AFRL.

II. Theory

2.1 Neutron Physics

A neutron is a neutral particle with a mass nearly equal to the mass of a proton and is the uncharged part of the nucleon pair [15]. Neutrons are commonly produced during nuclear reactions. When a neutron interacts with matter it can be penetrating but nonionizing. Because the neutron is nonionizing, it is difficult to detect using equipment and procedures designed for gammas, electrons or protons. Therefore, detection of secondary events of neutron initiated reactions is often necessary.

When a neutron interacts with matter it can be absorbed or scattered by the nucleus of that material. Absorption occurs when a neutron is captured by a nucleus or the nucleus fissions [8]. Neutron scattering can be elastic or inelastic and involves the neutron losing energy to the nucleus in the scattering collision. Elastic scattering occurs when the momentum and kinetic energy of the reaction are conserved. Elastic scattering presents itself in two ways. The first is when a neutron only interacts with the surface of the target [8]. The second is when the neutron is absorbed by the nucleus creating a compound nucleus. The compound nucleus then decays to the ground state of the resultant product nucleus. Inelastic scattering occurs when momentum is conserved but the kinetic energy of the neutron and nucleus is not conserved. Instead a photon is released. Essentially the compound nucleus decays to an excited state of the resultant product nucleus. The resultant product nucleus then releases energy via gamma photons to return to the ground state [8].

Neutrons are categorized based on their energy. Thermal neutrons are considered to be neutrons with an energy of 0.025 eV, or room temperature. Epithermal, slow and fast neutrons are considered to be those neutrons approximately in the 1 eV, 1 keV and 0.1 MeV and above range, respectively [15]. The probability of a neutron
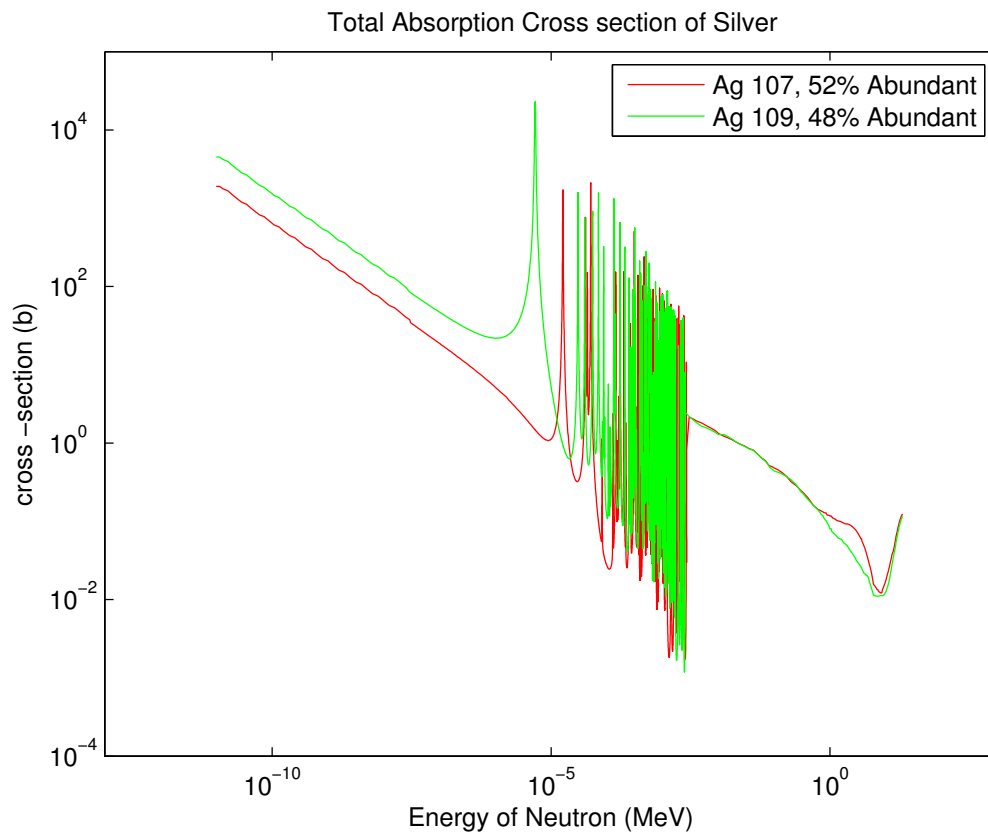
Figure 1. Silver absorption cross-sections from the ENDF library [2].

reaction with a nucleus is represented by neutron capture, fission, or scatter cross sections. A cross-section is the probability of a neutron being absorbed divided by the areal atom density (number of target atoms per unit area of the layer) [20]. The two silver isotopes found in natural silver present typical absorption cross sections as shown in Figure 1. The thermal region will follow a 1/v dependence, where v is the neutron velocity. For most elements, the cross-section will have a region of extreme variability in the epithermal and slow neutron regions. This region is called the resonance region. The extreme variability of the cross-section in the resonance region is due to the shell structure of the nucleus. Fast neutron energies typically have more steady cross-sections than those of the resonance region.

Neutron capture cross sections tend to be low in the fast region, therefore scattering is usually the dominant reaction. Moderation of a neutron occurs when the neutron scatters enough times to reduce its energy, increasing the probability of absorption, and is eventually absorbed. This could occur in one of the many resonances of the material or after the energy has reduced to the thermal region. To be an effective moderator the probability of a scattering interaction and the average energy loss in one scatter should be high. A particle will loose the most energy in a head-on collision with a particle of equal mass. Therefore, neutron-proton reactions should reduce a neutron's energy faster than any other material collision. Since the nucleus of ^{1}H is simply a proton, a material with an abundance of hydrogen will act as a very good moderator.

Measures of a good moderator include the moderating power and moderating ratios. The moderating power is

$$\xi\Sigma_s = \frac{\rho N_a}{M}(n_1\sigma_{s_1}\xi_1 + n_2\sigma_{s_2}\xi_2 + \cdots) \tag{1}$$

where ρ is the density of the compound, M is its molecular weight, N_a is Avagadro's

7

number, n_i is the number of atoms of element i in one molecule, σ_{s_i} is the microscopic scattering cross section of element i and ξ_i is the average logarithmic energy decrement for element i in a scatter

$$\xi_i = 1 - \frac{(A_i - 1)^2}{2A_i} ln\frac{(A_i + 1)}{(A_i - 1)} \tag{2}$$

where A is the element's atomic weight [20]. Polyethylene (CH_2) and water (H_2O) have an abundance of hydrogen are are considered to be good moderators. The moderating power of polyethylene for neutrons from 1 eV-100 keV is 3.26 compared to 1.28 for water [20]. The moderating ratio is given by the ratio of the scattering and absorption cross sections

$$\frac{\xi\Sigma_s}{\Sigma_a} = \frac{\rho N_a}{M}(n_1\frac{\sigma_{s_1}}{\sigma_{a_1}}\xi_1 + n_2\frac{\sigma_{s_2}}{\sigma_{a_2}}\xi_2 + \cdots) \tag{3}$$

where σ_{a_i} is the microscopic absorption cross section of element i [20]. A material with a high moderating ratio implies that material is a good moderator and poor absorber. The moderating ratio of polyethylene is 122 compared to 58 for water [20], which is why polyethylene is often chosen to moderate neutrons in detectors.

2.2   Fusion

Fusion is the process of combining two nuclei together to create a heavier nucleus. A typical nuclear reaction is written

$$a + X \rightarrow Y + b \tag{4}$$

where a and X are the particles that fuse, and Y and b are the reaction products [15]. This reaction is also commonly written X(a, b)Y. The energy difference, due to

8

mass, between the initial and final nuclei is the energy output, Q, of the reaction

$$Q = (m_{initial} - m_{final})c^2 = (m_X + m_a - m_Y - m_b)c^2. \tag{5}$$

where m_X and m_a are the rest masses of the particles that are fused, and m_Y and m_b are the rest masses of the reaction products [15]. When the Q values of a reaction is positive it releases energy. If the energy required to power a fusion reactor is less than the energy output of a sustained fusion reaction, it would be a viable alternative for energy production on earth.

Deuterium (D) is the ^{2}H isotope of hydrogen that is made of one proton and one neutron. It is abundantly found in the earth's oceans allowing for a nearly limitless supply of fuel for a fusion reactor. The four most probable ways that deuterium can fuse are

$$D + D \rightarrow {}^3He + n \qquad (3.27 MeV) \tag{6}$$

$$D + D \rightarrow T + H \qquad (4.03 MeV) \tag{7}$$

$$^3He + D \rightarrow {}^4He + H \quad (18.3 MeV) \tag{8}$$

$$D + T \rightarrow {}^4He + n \qquad (17.6 MeV) \tag{9}$$
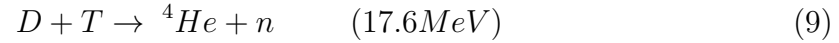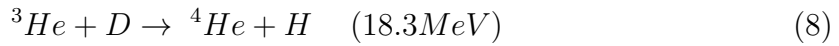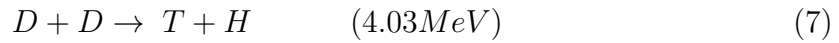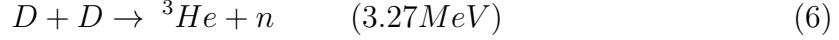
where D is a deuteron, T is a triton which is ^{3}H, and the Q value of the reaction is listed in parenthesis after the equation. Equations 6 and 7, show the two D-D reactions; the probability for either D-D reaction to occur is 50%. If a situation exists where deuterium is confined and begins to fuse, there is a high probability that both D-D and D-T reactions will occur. Therefore, neutrons of 2.45 MeV (from D-D reactions) and 14.1 MeV (from D-T reactions) may be observed from the confined fusion of deuterium.

Classically, in order for fusion to occur two ions must overcome the energy of the

Coulomb repulsion due to their positive charge. Equation 10 describes the amount of energy needed to overcome the Coulomb repulsion force of these nucleons [8].

$$E = \int_{\infty}^{R_b+R_t} \frac{Z_b Z_t e^2}{4\pi\epsilon_0 r^2} \, dr = -\frac{Z_b Z_t e^2}{4\pi\epsilon_0} \frac{1}{r}\bigg|_{\infty}^{R_b+R_t} \tag{10}$$

where

Z_b is the atomic number of the bombarding particle,

Z_t is the target nucleus,

e is the electric charge,

r is the separation distance of two charged nuclei,

ϵ_0 is the permittivity of free space, $8.85 \times 10^{-12} \frac{coulomb^2}{newton-m^2}$,

R_b is the radius of the nuclear force for the bombarding particle,

R_t is the radius of the nuclear force for the target particle.

R_b and R_t can be found from Equation 11

$$R = 1.25 \times 10^{-15} A^{1/3} \text{ m} \tag{11}$$

where A is the atomic mass number of the particle [8].

When Equation 10 is evaluated for the four deuterium reactions, the energy needed to overcome the Coulomb repulsion force is 381 keV, 381 keV, 355 keV and 711 keV for Equations 6, 7, 8, and 9 respectively [8]. The temperatures needed to obtain these energies are 10^7 times higher than room temperature (0.025 eV). However, Figure 2 shows that these fusion reactions occur at temperatures much lower than determined from Equation 10. This can be explained by the quantum mechanical concept of

10
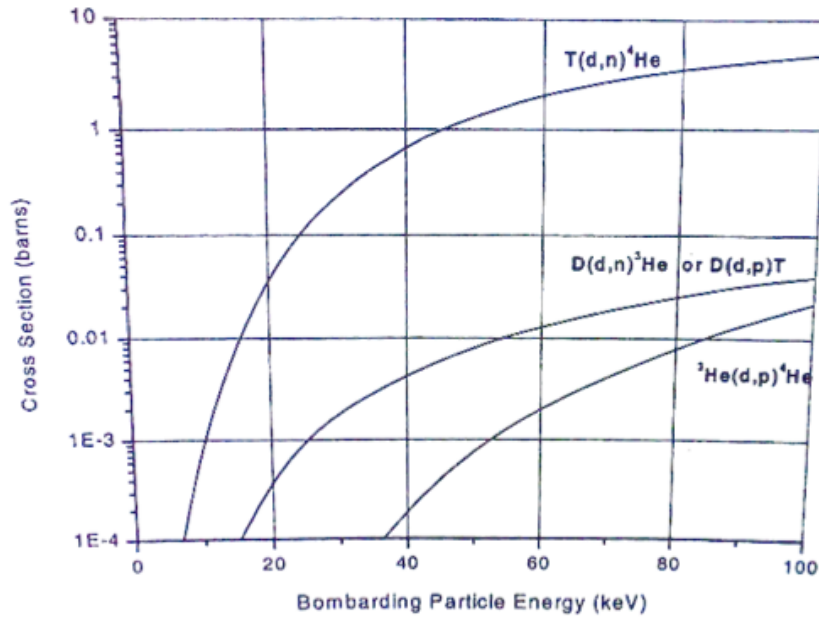
.
Figure 2. Fusion reaction cross-sections [8]

tunneling. Essentially, there is a probability determined by quantum mechanics that a particle will traverse the Coulomb barrier despite not having the required energy. This probability is represented by the cross-section of the fusion reaction. As shown in Figure 2, as the thermal energy of the system is increased, the cross-section and thus the probability of interaction increases. Also note that the D-T reaction is about 100 times more probable than the two D-D reactions. This is why deuterium confinement may produce neutrons from both D-D and D-T reactions.

Specific fuel conditions must be met before fusion will occur. Conditions including confinement time, density and temperature [17] will all factor into how much energy the gross yield of the many fusion reactions will release. A single fusion reaction will release the Q value of the reaction, or the amount of energy shown in parentheses in Equations 6 thru 9. Deuterium, for example, will be heated to a plasma state in order for fusion reactions to occur. The energy released from a plasma of a specific

11

density is given in Equation 12 [17].

$$E_{FUS} = Q\, n_0^2\, t\, \frac{\overline{\sigma v}}{4} \left(\frac{1}{1 + \frac{\overline{\sigma v}}{2} n_0 t} \right) \tag{12}$$

where

E_{FUS} is the fusion energy produced,

$\overline{\sigma v}$ is the average cross-section multiplied by the particle average velocity,

Q is the fusion reaction energy released from a single fusion event,

t is the elapsed time of the reaction, where $t = 0$ at the reaction start,

n_0 is the ion density at $t = 0$ [17].

Balancing the energy into the system to the energy out of the system, or achieving scientific breakeven, is the main goal of researching this method of energy for commercial use. Scientific breakeven is achieved when the fusion energy produced equals the initial plasma energy. Energy is lost to the environment through Bremmstrahlung radiation and thermal conduction, making scientific breakeven very difficult to achieve. The burn time necessary to achieve breakeven, while accounting for losses to the environment, means a longer plasma confinement time. The rate at which fusion energy is produced must be faster than the rate the energy is lost in order to have a sustained reaction. Independent of density, the minimum temperature required for a sustained reaction, thus achieving breakeven, occurs at 2.5 keV for D-D reactions and 3.5 keV for D-T reactions [8, 17].

The best system design minimizes energy loss to the environment. When the plasma is unmagnetized, the electron thermal conductivity dominates over ion thermal conductivity. Therefore, if the electrical conductivity is reduced the overall thermal conduction loss would be improved. Magnetizing the plasma causes the electrical

conduction to the walls to be reduced, which lowers the thermal conduction losses
[17].

When a plasma is embedded in a non-uniform magnetic field, and either the
plasma or the magnetic field move, an induced electromotive force will be generated
in the plasma according to Faraday's Law [18] as shown in Equation 13

$$EMF = -\frac{d\Phi_B}{dt} = -\int \frac{\partial \mathbf{B}}{\partial t} \cdot d\mathbf{A} \tag{13}$$

where Φ_B is the magnetic flux, $\mathbf{B}$ is the magnetic field and $d\mathbf{A}$ is the unit area
with the unit vector normal to and directed outward from the surface of integration.
Lenz's law states that there is a time when the induced current within the plasma
generated by the electromotive force is in such a direction that the magnetic field
generated by the current will oppose the change in magnetic flux which originally
caused the electromotive force. If the conductivity of the plasma is high enough
to induce currents and the magnetic fields are large enough changes in the external
magnetic field can be prevented [18]. The field lines are considered to be "frozen"
into the plasma when these conditions occur. As the plasma moves the field lines will
follow [18].

Another way to understand this concept is to consider how the magnetic flux
changes with time. Consider a magnetic flux that moves through a contour C, which
is co-moving with the plasma [10]. The time variation of the magnetic field, $\mathbf{B}$, over
a surface, S, which spans C can be written as

$$\frac{d\Phi_B}{dt} = \int_S \mathbf{B} \cdot d\mathbf{S}. \tag{14}$$

In addition to Equation 14, the magnetic flux also changes due to the motion of C as

13

shown in Equation 15

$$\frac{d\Phi_B}{dt} = \int_C \mathbf{B} \cdot \mathbf{V} \times d\mathbf{l} = \int_C \mathbf{B} \times \mathbf{V} \cdot d\mathbf{l} \tag{15}$$

where $\mathbf{V}$ is the flow velocity, and $d\mathbf{l}$ is an element of C. $\mathbf{V} \times d\mathbf{l}$ is the area swept out by $d\mathbf{l}$ per unit time [10]. By applying the Faraday-Maxwell equation to Equation 14 and Stokes's theorem to Equation 15 and combining both, the time variation of the magnetic field is obtained as shown in Equation 16

$$\frac{d\Phi_B}{dt} = -\int_A \nabla \times (\mathbf{E} + \mathbf{V} \times \mathbf{B}) \cdot d\mathbf{A}. \tag{16}$$

When $\nabla \times (\mathbf{E} + \mathbf{V} \times \mathbf{B}) = 0$ and therefore when $(\mathbf{E} + \mathbf{V} \times \mathbf{B}) = 0$ the frozen-in flux condition exists [10].

When the fusion fuel becomes a plasma and is magnetized, achieving a plasma with frozen-in field lines is the goal. A high temperature (and therefore velocity) plasma will have a magnetic field that is frozen in place. When the plasma is compressed with a frozen-in field the magnetic field will also be compressed. The magnetic field can increase to the Megagauss range through this compression. The fusion plasma will ignite and sustain a burn if the plasma self-heats, meaning the byproducts of the fusion deposit energy in the plasma. The critical parameter to self-heating is the gyroradius shown in Equation 17

$$r_c = \frac{mv}{qB} \tag{17}$$

where m, v, and q are the mass, velocity, and charge of the fusion byproduct and B is the magnitude of the magnetic field [13]. When the gyroradius is "much smaller than the fusion plasma radius, a significant part of the energy of charged fusion products will be deposited to self-heat the plasma" [13].

Additional benefits to magnetizing the plasma are a smaller burning plasma size,

14

reduced energy and reduced implosion velocity requirements to compress the plasma [17]. The minimum fusion system size is a function of density, temperature and magnetic field [17]. Once the size is determined, the minimum fuel mass, plasma energy, required heating rate and intensity, and ultimately the implosion velocity can be determined. Because minimum size is a function of the magnetic field, when the fuel is magnetized the size is significantly reduced. Once the size is reduced enough the energy required for the reaction is also reduced to the megajoule range; enough to utilize the energy production of pulsed power facilities such as Shiva Star.[17].

2.3   Magnetized Target Fusion

Magneto Inertial Fusion (MIF) is an approach that uses the idea of magnetizing a plasma to enhance particle and energy confinement [11]. Magnetized target fusion is a type of MIF that "compresses the plasma target with closed magnetic surfaces, and adiabatic heating to fusion relevant conditions inside of a converging and flux conserving boundary (e.g. liner)" [11]. AFRL's Shiva Star facility is working on the Field Reversed Compression and Heating Experiment (FRCHX) which is a design based on the high density field-reversed configuration experiment system designed by LANL. The FRCHX forms a Field-Reversed Configuration (FRC) plasma, translates this plasma into a cylindrically symmetric aluminum "liner" which is then radially compressed [11]. Figure 3 shows a schematic of the FRCHX. The magnetized plasma is formed in the theta coil, it is then translated vertically through the guiding coils into the aluminum liner where it is trapped by the magnetic mirror created by the upper and lower mirror coils. The current pulse transmission lines from the Shiva Star capacitors feed at the top of the liner to power the device [11]. Magnetohydrodynamic simulations of the plasma FRC formation, translation and liner compression have been done using the MACH2 MHD program [26]. The Shiva Star capacitor bank couples

15
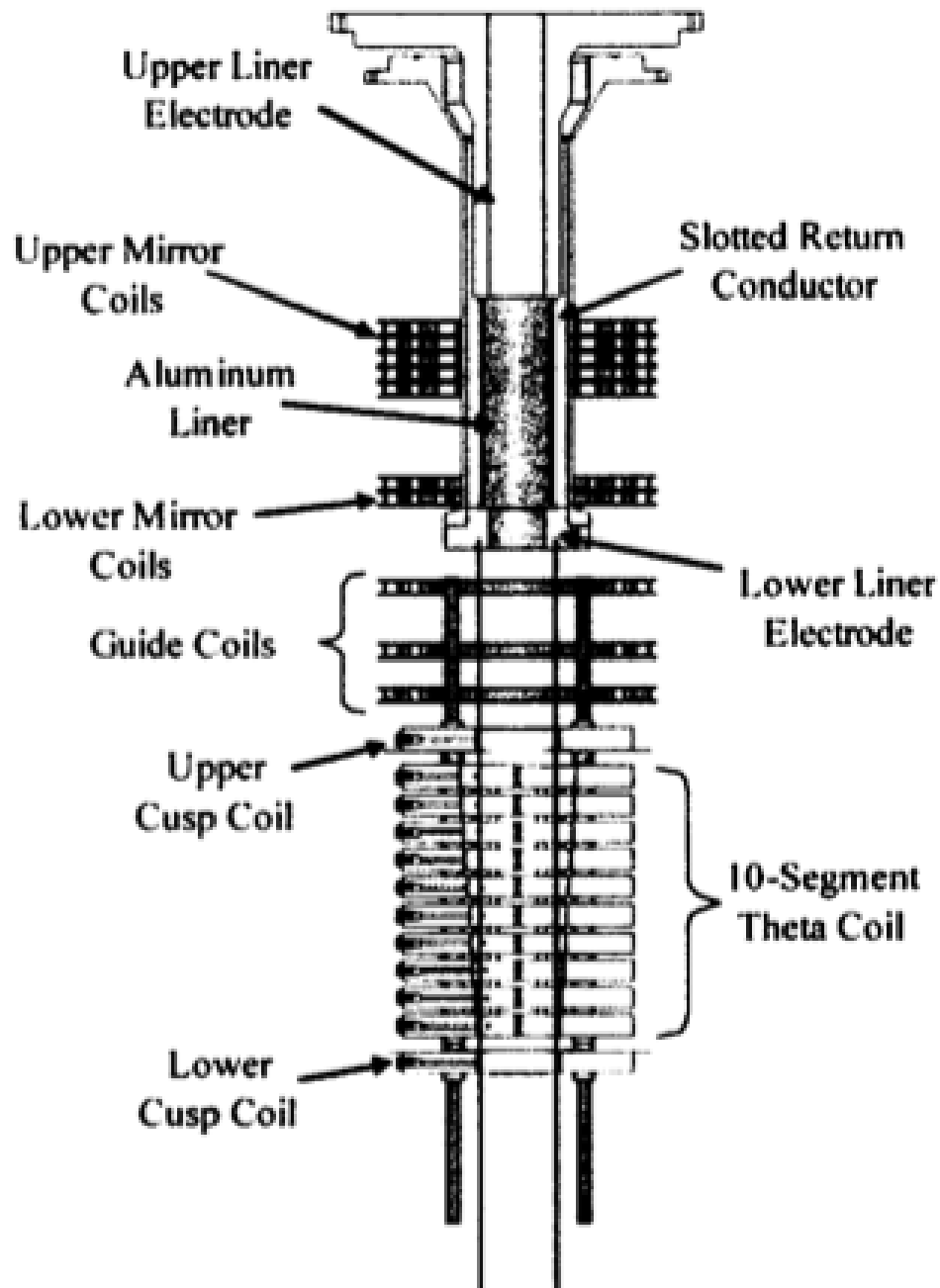
Figure 3. Schematic of the FRCHX. The magnetized plasma is formed in the theta coil, it is then translated vertically through the guiding coils into the aluminum liner where it is caught by the magnetic mirror created by the upper and lower mirror coils. The current pulse transmission lines from the Shiva Star capacitors feed at the top of the liner to power the device [11]

approximately 1.5 MJ of kinetic energy into the aluminum liner, which collapses cylindrically at an implosion velocity of approximately 5 km/sec. Initial MACH2 calculations predicted that the FRCHX experiment would produce a d-d neutron yield of 10^{12}, with a plasma density of 5×10^{18} ions/cm^3 and a temperature of 5 keV [26].

To measure any one type of radiation quanta during a neutron burst is difficult due to all of the background reaction byproducts. Narrowing the search for neutrons requires a detector that is gamma insensitive because those detectors that can measure secondary neutron reactions are designed to also measure gamma photons. Many ionization detectors suffer pileup, causing the detector to essentially be dead for a period of time. This "dead time" can last as long if not longer than the entire source neutron burst time length. Therefore, having a detector that is insensitive to the time length of the neutron burst is also important. Using a neutron activation detector to measure the neutron burst once the burst ends eliminates both the inadvertent measurement of fusion byproducts as well as the burst time length concerned. This is why a neutron activation detector was chosen by AFRL to measure neutrons for the FRCHX experiment. The research at AFIT will use an AFRL silver detector to measure the neutron activated silver decays from the neutrons of the neutron burst with a known neutron yield to determine a calibration factor. Ultimately, this calibration factor will be useful in determining the neutron yield from the FRCHX fusion burst based on the measured counts from the silver detector.

2.4 Silver Detector

AFRL uses two silver detectors based on the design schematics of the Lanter & Bannerman paper [16] to count neutrons from the fusion reaction in the FRCHX experiment. The Lanter & Bannerman based silver detector is comprised of four

Geiger-Müller (G-M) tubes that are wrapped in silver foils and surrounded by a single polyethylene block. The fast neutrons from the plasma reactions are moderated in the polyethylene block. The moderated neutrons are captured by the silver creating a radioactive isotope which then beta decays. This beta interacts with the G-M tube, creates a signal that is detected by the electronics, and is counted using a counter/timer. Gammas are produced during the moderation process in the neutron reactions with the polyethylene, as well as from neutron inelastic scatter events in the silver. These gammas could interact with the G-M tubes, however they will have traveled out of the system by the time the detector begins measuring the beta decays from the silver activated foils because the measurement occurs after the burst of neutrons.

2.4.1 Natural Silver

The silver foil used in the silver detector is formed of natural silver. Natural silver consists of 51.8% ^{107}Ag and 48.2% ^{109}Ag. There are four possible neutron capture reactions from these two isotopes [3, 6, 21]. Equations 18 and 20 are the equations of interest for this research.

$$^{107}Ag + n \xrightarrow{\sigma_{n_{th}},\gamma=37\pm2b} {}^{108}Ag \xrightarrow{97.15\%} {}^{108}Cd + \beta^- + \nu \tag{18}$$

$$^{107}Ag + n \xrightarrow{\sigma_{n_{th}},\gamma=0.35b} {}^{108m}Ag \xrightarrow{91.3\%} {}^{108}Pd + \epsilon \tag{19}$$

$$^{109}Ag + n \xrightarrow{\sigma_{n_{th}},\gamma=89\pm4b} {}^{110}Ag \xrightarrow{99.7\%} {}^{110}Cd + \beta^- + \nu \tag{20}$$

$$^{109}Ag + n \xrightarrow{\sigma_{n_{th}},\gamma=4.7\pm4b} {}^{110m}Ag \xrightarrow{98.64\%} {}^{110}Cd + \beta^- + \nu \tag{21}$$
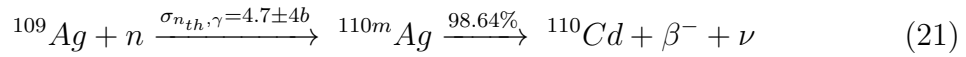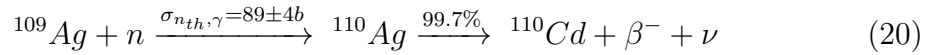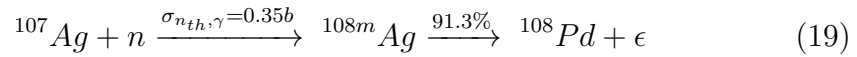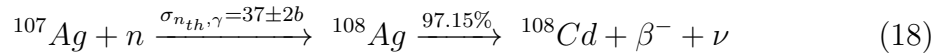
The ^{108}Ag isotope has a 2.38 minute half-life and decays with a maximum beta of 1.65 MeV. The ^{110}Ag isotope has a 24.6 second half-life and decays with a maximum beta of 2.89 MeV [16, 27, 21]. The half-lives for the ^{108m}Ag and ^{110m}Ag are 438 years

and 252 days, respectively [6, 21]. The National Nuclear Data Center (NNDC) decay schemes of ^{108}Ag and ^{110}Ag are shown in Appendix D. The ^{108}Ag and ^{110}Ag isotopes beta decay to the respective cadmium ground state 95.5% and 94.9% of the time, respectfully [21]. This means that only about 5% of the time the cadmium will be formed in an excited state, thus emitting a gamma ray. The gammas that will be emitted as a result of a reaction products excited states could interact with the G-M tube during the measurement timeframe. However a correction for these gamma reaction will be ignored due to the low percentage of formation.

2.4.2 Silver Detector Description
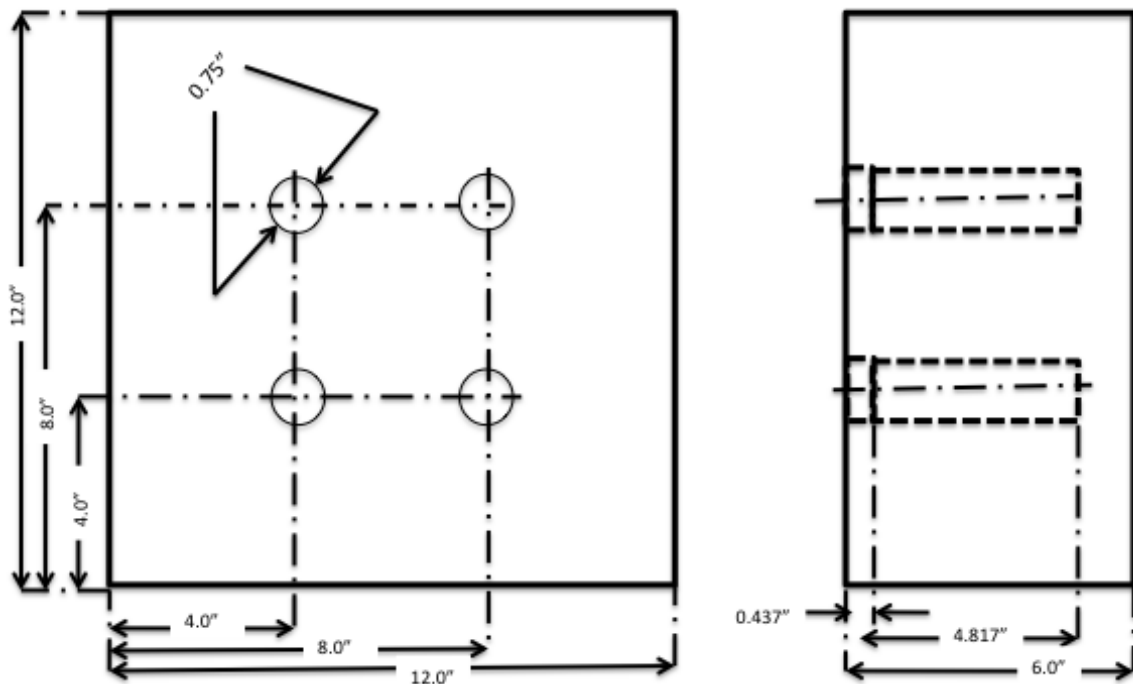
Figure 4. Schematic of silver detector described by the 1966 paper by Lanter and Bannerman [16] used by AFRL to design their silver detectors.

The silver detector is a 12" × 12" × 6" block of polyethylene containing four G-M

19

tubes wrapped with a 10 mil (0.254 mm) thick silver foil. A schematic of the silver detector as described by the 1966 Lanter and Bannerman paper is shown in Figure 4. Figure 5 shows the electronic set up of the counting experiment. The four signals are summed at a solder joint and brought to a bias-T. The DC portion of a high voltage bias supply is connected to the bias-T which powers the G-M tubes. The G-M output signal travels thru the bias-T, to a linear amplifier and then to a counter/timer for data collection [24].
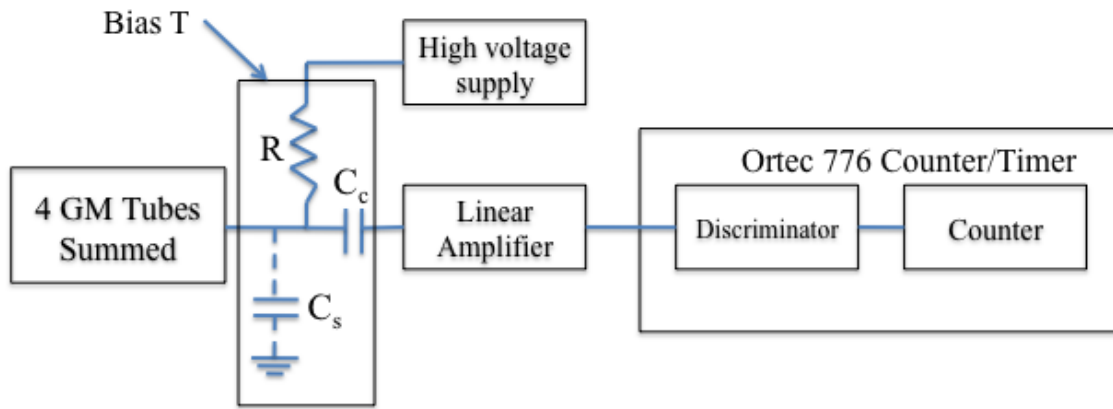
Figure 5. Block diagram of the electronics used in this experiment. A 1MΩ resistor and two .005 μF capacitors are used. The C_c is the coupling capacitor which blocks the high voltage, allowing the signal from the G-M to to be transmitted to the rest of the electronics [14]

2.4.3 Geiger Müller Tubes

When a neutron is captured by a silver atom (resulting in the reactions shown in Equations 18 and 20) the silver is considered to be activated by the neutron. The beta particles enter the G-M tube wall ultimately reaching the G-M tube gas. Figure 6 is a schematic of a side window G-M tube which is suitable for beta-gamma counting

20
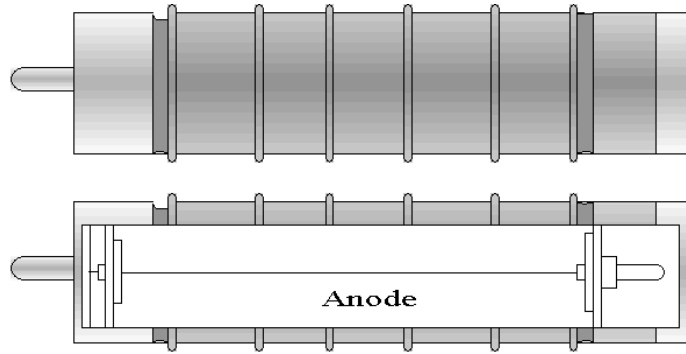
Figure 6. Thin-walled, side window G-M tube. The wall is the cathode, and the thin wire is the anode. The gas is inside the tube surrounding the anode wire. [4]

because of its thin wall which allows the electron to penetrate into the detection gas. The anode wire is in the center of the tube, surrounded by a low-Z gas, enclosed by the cathode wall. When a charged particle or photon deposits enough energy into the gas, the gas is ionized. The G-M tube is held at a high potential creating a large electric field that sweeps the free electrons towards the anode wire and the ions towards the cathode wall.

An electron gains enough additional kinetic energy from the electric field to increase its energy above the neutral gas ionization energy creating more electron-ion pairs. Thus a chain reaction, or avalanche, is created in the area of the anode wire [14] as shown in Figure 7. The ions have a significantly smaller mobility than the free electrons, and are much slower in reaching the cathode wire. The free electrons are absorbed by the anode wire before the ions have moved any substantial distance. The avalanche is stopped when the positive charge from the ions is large enough to reduce the magnitude of the electric field near the anode wire. Thus the energy of the free electrons decreases below the necessary level to further ionize the gas [14].
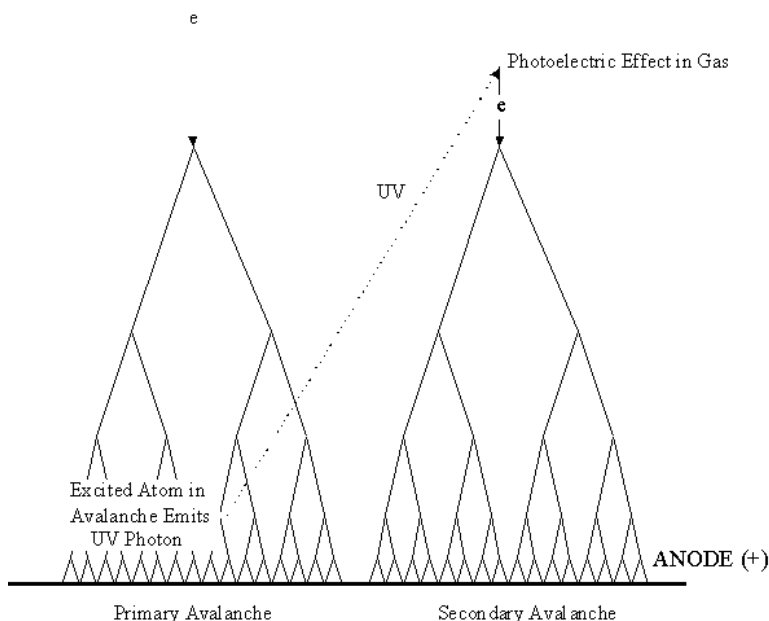
Figure 7. A schematic of an avalanche created by a single beta event. A UV photon is released by one of the reactions causing a new avalanche to occur further down the wire. [4]

2.4.4 Neutron Activation

The normal method of neutron activation detection involves irradiating a foil and then transferring that foil to a detector, such as a high-purity germanium detector, for measurement of the decaying isotopes. The act of moving the foil to the detector institutes a delay between the time the foil was removed from the radiation to the time counting begins. The silver detector has a silver foil directly in contact with its detectors, the G-M tubes. There is a time delay associated with this method of measurement as well. However, instead of removing the foil from the vicinity of the source, the source is removed from the vicinity of the foil. The time delay spans the time after the neutron burst ends to the time the measurement begins.

During the FRCHX experiment, the time between the end of the neutron burst and measurement is small (a fraction of a second). The flash and noise are seen and heard from the fusion explosion and the operator turns the detector on. However,

22

for the research conducted at AFIT, the time between the end of the neutron burst and the measurement is on the order of seconds. During the delay time between the neutron burst and the measurement, the activated nuclei begin to decay. The number of counts measured by the detector in a given time period after the source has been removed can be determined if the activity of the source, the half-life of the source, and background are known, as shown in Equation 22

$$C = \epsilon \int_{t_1}^{t_2} A_0 e^{-\lambda(t-t_0)} dt + B \tag{22}$$

where A_0 is the activity of the silver foil at the time the neutron burst ends, ϵ is the detector efficiency, λ is the decay constant, B is the background and C is the counts observed in the time interval from t_1 to t_2. The decay constant can be found by

$$\lambda = \frac{ln\,2}{t_{1/2}} \tag{23}$$

where $t_{1/2}$ is the half-life of the isotope [14]. The intrinsic efficiency is found by determining the ratio of signals recorded by the detector to the radiation quanta incident on the detector. Equation 24

$$\epsilon_{int} = \frac{N}{S}\frac{4\pi}{\Omega} \tag{24}$$

describes the efficiency in terms of the number of source quanta, S, and the number of counts measured, N, in a given time frame, and the solid angle subtended by the detector at the source position, Ω. The absolute efficiency is determined using

$$\epsilon_{abs} = \frac{N}{S} \tag{25}$$

where N is the number of counts recorded by the detector and S is the number of

radiation quanta emitted by the source. In the case of the silver foil/G-M tube absolute efficiency, the S would be the neutron activated byproduct decay for the entire silver foil. For the silver foil/G-M tube intrinsic efficiency, the S term would be those neutron activated byproduct decays that are incident on the G-M tube surface.

Figure 8 shows the activity of a typical neutron activation foil as a function of time. In this figure, the foil is exposed to a constant neutron source at time $t = 0$ and the source is removed at time t_0. Counts are measured between t_1 and t_2 and are represented by the shaded area under the curve. The activity of the foil at t_0 can be determined using the measured counts, C, from t_1 to t_2 and integrating and rearranging Equation 22 into Equation 26
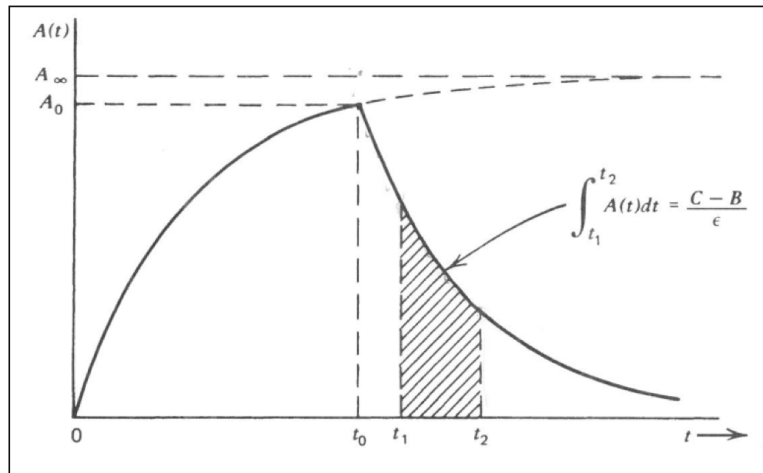
Figure 8. The activity of a foil activated by a neutron flux over time. The foil is exposed to a neutron flux at time $t = 0$ and removal at time $= t_0$. A detector used to measure the decays from the activated foil measure the number of counts which is proportional to the area under the decay curve between t_1 and t_2. [14].

$$A_0 = \frac{\lambda(C - B)}{\epsilon \, (e^{\lambda t_0})(e^{-\lambda t_1} - e^{-\lambda t_2})}. \tag{26}$$

For natural silver, the decay constant, λ, is a weighted value as shown in Equation

24

$$\lambda = 0.31 \ \lambda_{^{108}\mathrm{Ag}} + 0.69 \ \lambda_{^{110}\mathrm{Ag}} \tag{27}$$

where $\lambda_{^{108}\mathrm{Ag}}$ is the decay constant for $^{108}\mathrm{Ag}$ and $\lambda_{^{110}\mathrm{Ag}}$ is the decay constant for $^{110}\mathrm{Ag}$. The weight values are determined from the isotopic ratio present in the material as a whole as well as the cross-section of that isotope to thermal neutron capture. A calculation of these values is shown in Appendix B.

III. Experiment

3.1 Lanter and Bannerman

A paper written by Lanter & Bannerman [16] provided design and calibration information for the specific type of silver detectors that were manufactured by AFRL for the FRCHX experiment. In this paper, an initial calibration is described using the Cockcroft-Walton accelerator in pulsed mode which produced neutrons via a D-D reaction. A 200 μA beam of 250 keV deuterons bombarded a deuterated zirconium target [16]. A proton counter with a sensitivity of 3.86×10^4 neutron per proton count was used to count the protons from D-D fusion as in Equation 7. The beam was pulsed once for 0.3 seconds creating a burst of 10^8 neutrons [16].

The silver detector counted neutrons from the source at distances of 2.25", 6", and 12". The detector was used to measure the number of signals produced in a one minute interval after the burst. The observed count of signals, C, was used to determine the true count, C_t, of neutrons in the one minute interval explicitly by

$$C_t = \frac{2.7 \times 10^5 (\, e^{\, 2.69 \times 10^{-6} \, C} - 1)}{1 - 0.276 \, e^{\, 2.69 \times 10^{-6} \, C}} \tag{28}$$

C_t incorporated the resolution time of the G-M tube and the effective decay constant of the two silver isotopes. Table 1 shows that adjusting the observed counts only makes a 1% difference when the observed counts are above 2,500 counts per minute. Details of this derivation can be found in Appendix 3 and 4 of the Lanter & Bannerman paper [16].

The neutron yield for an unknown burst of neutrons can be found using a calibration factor for a known source. A calibration factor (F_{dd}), as shown in Equation 29, is determined using a known source neutron yield (N), and the true counts (C_t)

Table 1. The results of the observed counts, C, compared with true counts, C_t, from the work by Lanter & Bannerman. C_t was determined by using Equation 28. It can be seen that observed counts below 2500 per minute are changed by less than 1% when converted to true counts. Therefore, corrections to counts below 2500 per minute were determined to be negligible. [16]

C	C_t	C_t/C
2500	2525	1.01
10000	10300	1.03
25000	26,750	1.07
50000	56600	1.13
75000	90000	1.20
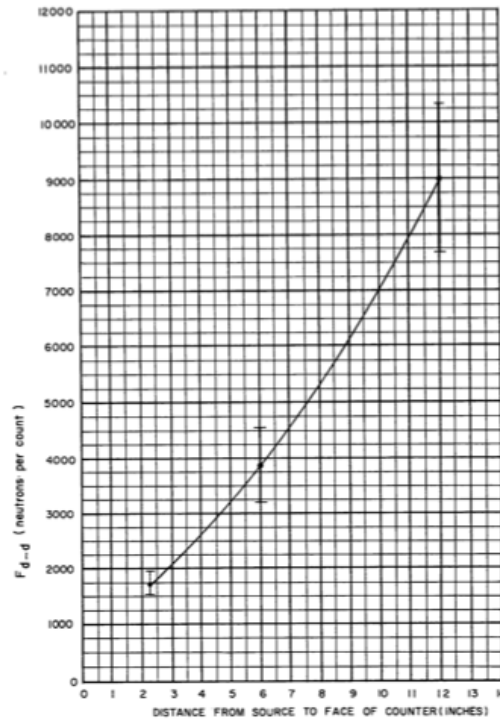
Figure 9. This is the calibration factor from the Lanter & Bannerman paper for D-D neutrons with respect to distance from the source to the moderator. [16]

27

measured by the detector

$$F_{dd} = \frac{N}{C_t}. \tag{29}$$

Lanter and Bannerman determined the calibration factor based on the counts measured at three distances. The calibration factor was graphed as a function of distance and is shown in Figure 9. The best fit line connecting the points shown in Figure 9 was determined using a square law curve [16]

$$F_{dd} = 30(5.3 + D)^2, \tag{30}$$

where D is the distance in inches between the source and the front face of the silver detector. The neutron yield of an uncalibrated pulsed source can be found using

$$N = F_{dd}\, C_t. \tag{31}$$

When AFRL was manufacturing the silver detectors to be used on the FRCHX experiment, the Victoreen 1B85 G-M tubes used by Lanter and Bannerman could not be obtained. The 1B85 tubes were aluminum walled and filled with argon and an organic quenching gas. The tubes used by AFRL use a 446 stainless steel wall with neon and a halogen quenching gas. Lanter and Bannerman did a study of G-M tubes to determine that as long as the resolution time of the average of the four G-M tubes equaled 125 ± 10 μs their calibration factor could still be used [16]. However, due to the G-M tube change in the AFRL manufactured silver detectors, the calibration data obtained by Lanter and Bannerman would not be accurate. Therefore, AFRL determined a new calibration factor for the silver detectors.

For the AFRL calibration experiment, the detectors were placed in the FRCHX test area at Shiva Star. Using a D-D neutron generator with an estimated strength of 10^7 n/s, five measurements were taken, three at 40.6" and two at 44" [24]. The number

of counts observed was less than 2500 and therefore the observed counts, corrected for background, were taken to be equal to the true counts. The neutron-per-second output of the neutron generator was only estimated, therefore, the neutron yield for the AFRL measurements were found using Equation 30. The Findfit function of the mathematical computational program called Mathematica [25] used the neutron yield, counts, and distance to determine a calibration factor of the same form as Lanter and Bannerman's calibration factor. Findfit uses a least squares method to determine the best fit equation based on a user defined form. The code for this can be found in Appendix E. A function of the same form as Equation 30 was found to be

$$F_{D-D} = 55.6(9.5 + D)^2 \tag{32}$$

where D is the distance in inches between source and the front face of the silver detector.

Because the neutron yield of the source used for the AFRL calibration was not actually known and there is a four order of magnitude difference between neutrons expected and neutrons measured from the FRCHX experiment, a question as to the validity of the calibration has been posed. Therefore, a new calibration using a source with a known neutron activity was performed in this research effort.

3.2 Source Selection

MCNP simulations were used to determine if a PuBe source could replicate the spectrum of neutrons that reach the silver foils of the silver detector from a D-D fusion source. A point source with the energy distribution of a typical PuBe spectrum shown in Figure 10 was used in the MCNP simulations. The geometry used in the MCNP simulations are shown in Figure 11. The polyethylene rectangular parallelepiped was
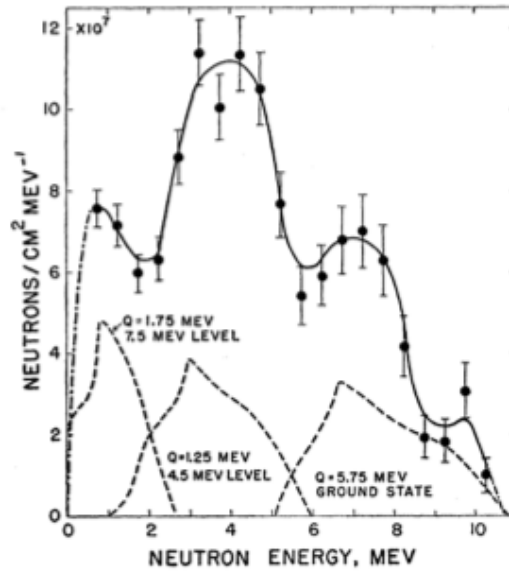
Figure 10. Energy spectrum of neutrons generated from a PuBe source.[22]
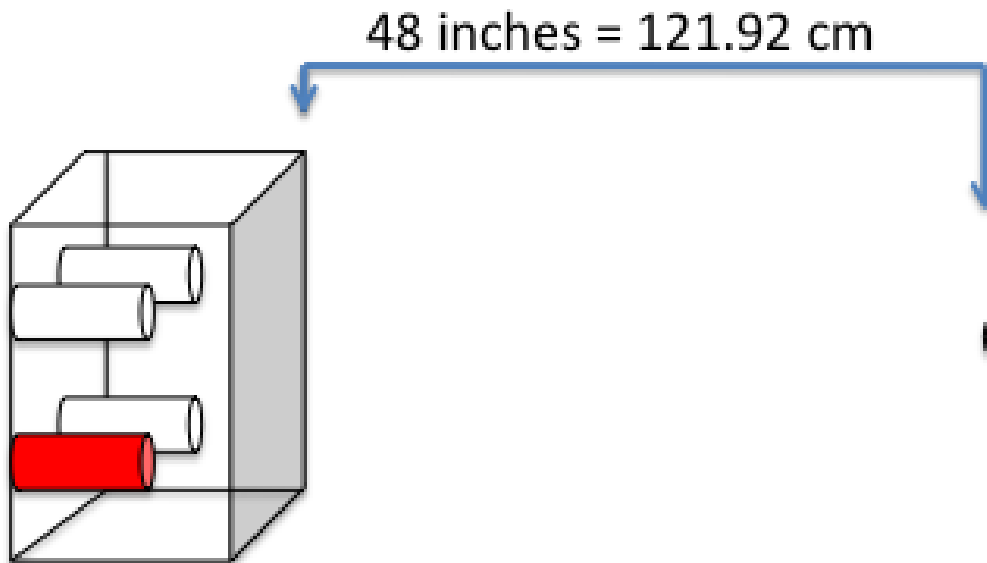
Figure 11. MCNP geometry with the polyethylene block. The red cylinder represents the bottom right GM tube, the tube that is used to compute the MCNP tally information.

created with four cylinders inside the parallelepiped representing the G-M tubes. Each tube consists of a cylinder of neon, stainless steel and silver in increasing diameter representing the neon fill gas and the stainless steel wall of the G-M tube as well as the silver foil that is wrapped around the G-M tube. The source was placed 48 inches from the front face of the polyethylene. The normalized neutron flux from the PuBe source was determined using four flux tallies, one at each of the four silver foils.

The spectral outputs of the four MCNP F4 neutron flux tallies are displayed in Figure 12 where the neutron energy is shown on the x-axis and the normalized neutron flux $(1/cm^2)$ in the silver foil is shown on the y-axis. The F4 tally computes the average neutron track length in a cell per source particle [9]. The energy bin structure for the MCNP simulations was the same as that used in the ENDF cross-sections shown on the x-axis in Figure 1. Figure 12 shows the neutron flux in any of the four silver foils is approximately the same regardless of the foil location. To show this more clearly, Figure 13 is a plot of the relative differences between the normalized neutron flux at the different silver foil locations compared to the flux at the bottom right detector location. The differences are taken relative to the bottom right (BR) detector that is shown in red in Figure 11. BR, BL, TR, TL represent bottom right, bottom left, top right and top left detector locations, respectively. As shown, the differences between the four spectra are an order of magnitude less than the normalized neutron flux. This indicates that all four silver foils receive the same energy dependent flux and therefore, only one tally location can be used to save on computational time.

The FRCHX uses a D-D fusion source. Therefore a comparison of the energy dependent neutron flux at the silver foils for a D-D source and a PuBe source is necessary if the intent is to use the AFIT calibration for the FRCHX experiment. The MCNP model used a 2.45 MeV monoenergetic, isotropic neutron point source

31
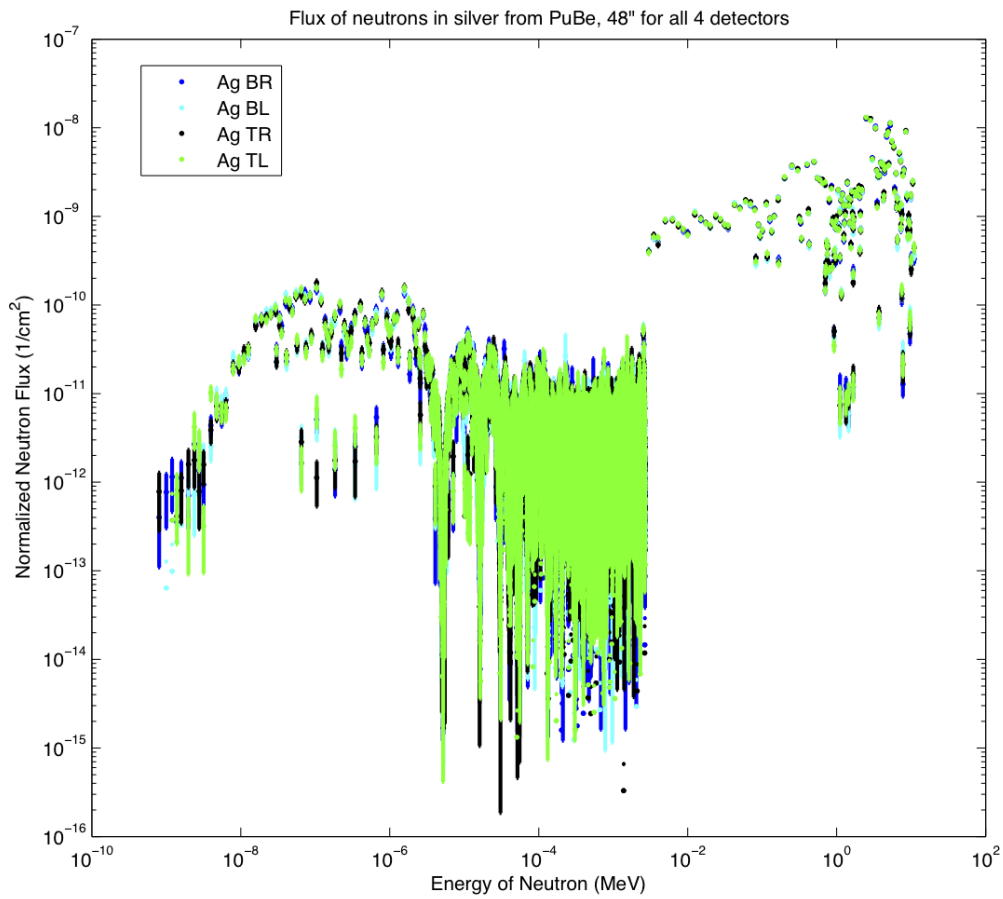
Figure 12. Flux spectra at each of the silver foils surrounding each for the G-M tubes, 48" away from the PuBe source.
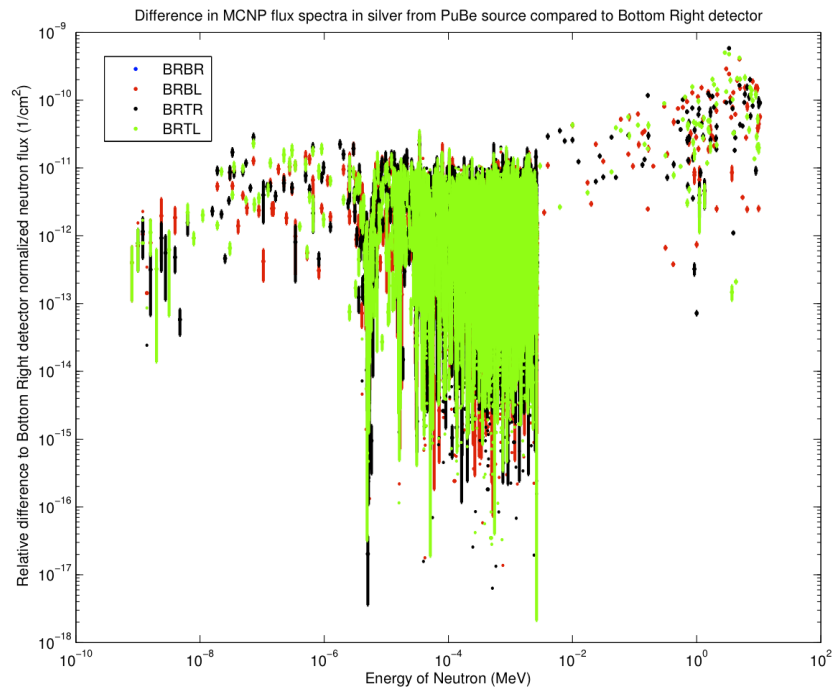
Figure 13. The relative difference in MCNP spectra output of each of the four detectors compared to the output of the bottom right detector. The spectra compared are those shown in Figure 12.

to simulate a D-D fusion neutron spectral output. Figure 14 shows the normalized
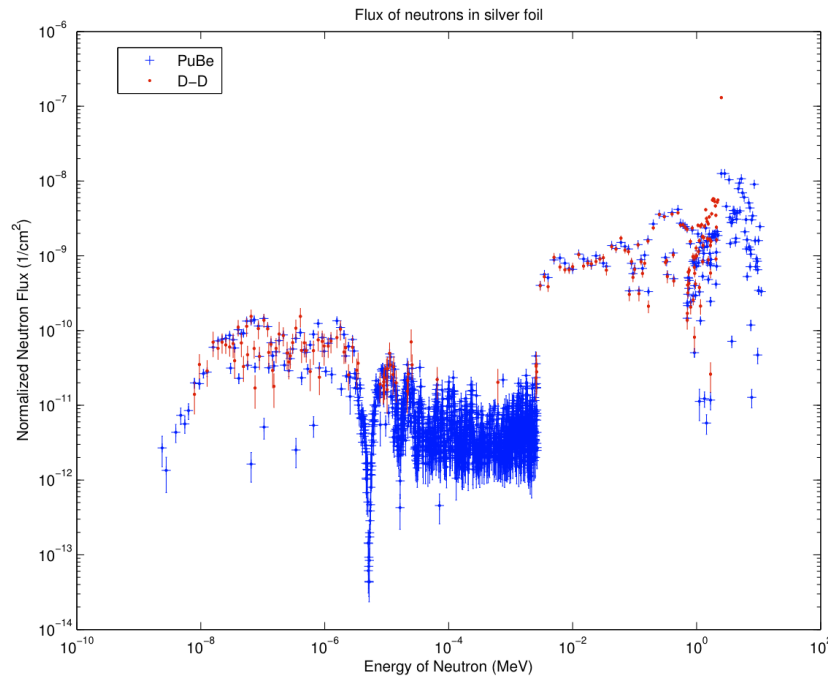
Figure 14. 48" normalized neutron flux data where the MCNP relative error was less than 0.5.

neutron flux distributions from the simulated D-D fusion and the simulated PuBe source at the bottom right silver foil 48 inches away from the source. All 10 statistical checks passed for both data sets, however, some of the points had relative errors that were considered irrelevant by the MCNP manual [9] and were disregarded prior to plotting. The large errors on numerous points was due to low counting statistics caused by the 48" distance between source and detector with no variance reduction techniques applied to the simulation.

To compensate for this, another MCNP simulation was developed for both sources 2.25" away from the detector. All outputs from the 2.25" and 48" simulations are shown in Figure 15. All statistical checks passed for the 2.25" simulation of the D-D

34

www.manaraa.com
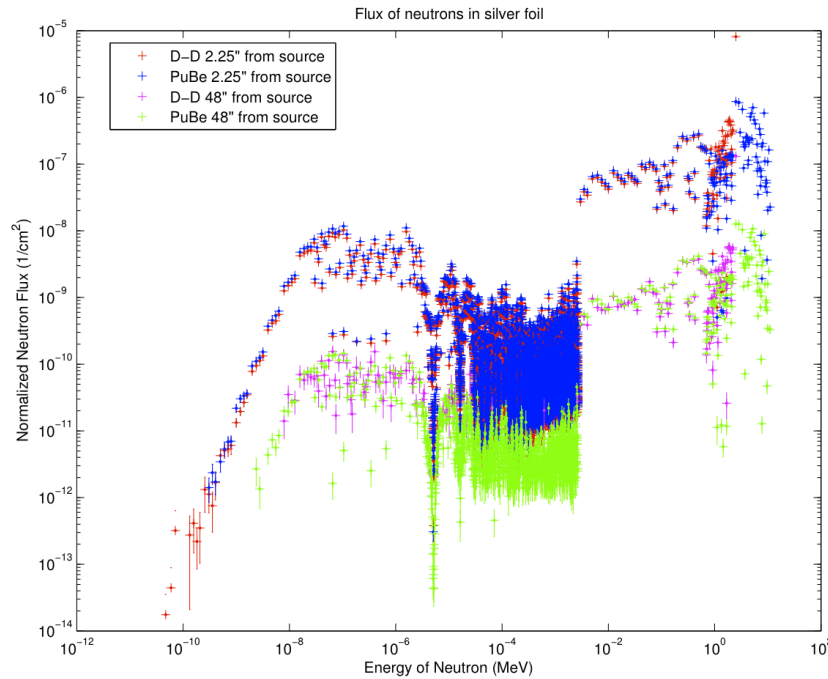
Figure 15. PuBe vs D-D MCNP spectra comparing 48" an 2.25" from source.

source. However, the statistical check requiring the figure of merit to be nonmonotonic in the last half of the problem for the 2.25" simulation of the PuBe source did not pass. Points were disregarded if they had a relative error greater than 0.5. For all data there is a jump in neutron flux around 10^{-2} MeV because the energy bin size increases from steps on the order of 10^{-7} to 10^{-3}. Therefore, more neutrons are being counted in one bin compared to previous bins. There is a large spike at 2.45 MeV in the two D-D specta due to the MCNP response of simulating a monoenergetic point source. The PuBe distributions have source energetic neutrons above 2.45 MeV which is why there is a normalized neutron flux shown in energy bins greater than 2.45 MeV for the PuBe source.

The relative difference between the PuBe spectrum and the D-D spectrum for the both the 2.25" and 48" simulations is shown in Figure 16. The difference between the two spectra 2.25" away show an normalized flux an order of magnitude smaller
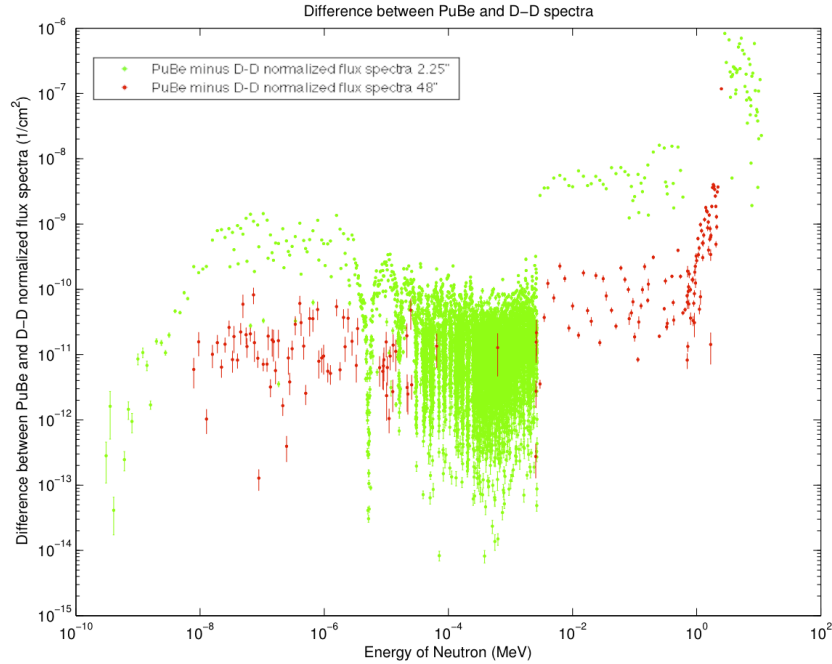
Figure 16. Relative difference of PuBe to D-D MCNP spectra.

than the original spectra for all points. However there are some points in the thermal region of the 48" difference spectra that are the same order of magnitude as that of the original spectrum. These points also have large errors associated with them. Because the spectrum shape looks the same for both the 2.25" and 48" MCNP simulations, it is safe to say that the if the counting statistics were increased, the 48" thermal region would show a similar order of magnitude difference as that shown for the 2.25" simulations. Therefore, the PuBe source and the D-D source have the same flux in the silver foil within the same order of magnitude in the thermal region. The normalized flux is multiplied by the microscopic cross section for each energy bin and is shown in Figure 17. The thermal region has the highest probability of having an absorption reaction. Ag 109 has a very prominent resonance at about 10^{-5} MeV which is comparable to the probability of reaction in the thermal region. The thermal cross section will be used in calculations during this research. For future work, an

36
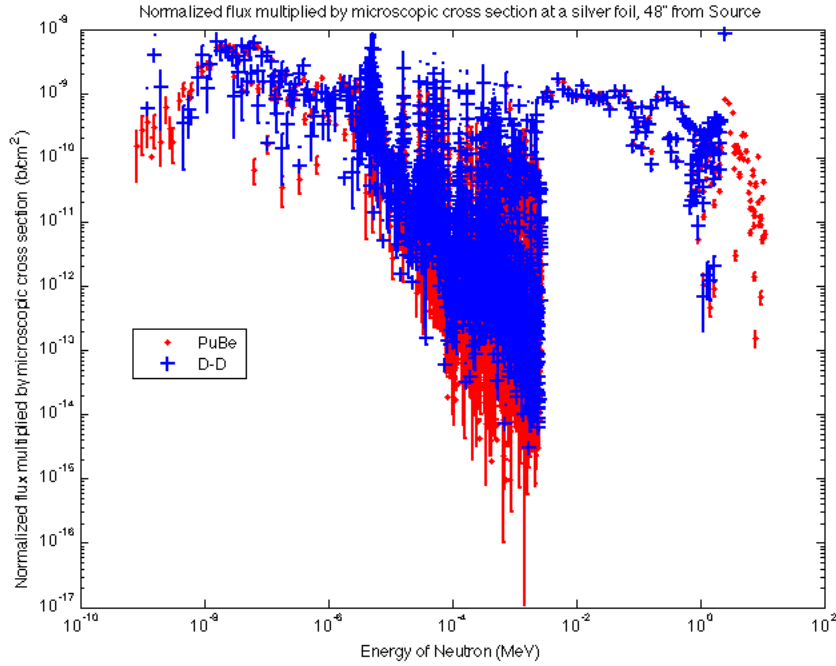
Figure 17. Normalized flux multiplied by the microscopic cross section at a silver foil

analysis to determine the necessity of incorporating the resonance cross sections into the calculations should be considered.

3.3 AFIT PuBe Source

A calibration factor for the silver detectors can be found if a source with a known activity is used. The PuBe source that was used for this research had been recently calibrated to account for the ^{241}Am buildup that has occurred over the lifetime of the source. Information about the source is shown in Table 2. The recent calibration used foil activation of Au, In, and Cd to determine the neutron spectrum. The activity of the foils were corrected for timing, resonance escape, flux depression and self-absorption affects. The Sources 4C computer modeling code determines neutron production rates due to radionuclide decay [23]. Using Sources 4C it was determined that the source strength was $1.01 \pm 0.01 \times 10^7$ neutrons per second and that there

was no appreciable change in the neutron energy spectrum due to the increase of ^{241}Am [7].

Table 2. PuBe source used during this experiment

Inital Activity	4.685 Ci
Date of Initial Activity	09 Mar 1962
Manufacturer	Monsanto
Rate of Neutron Production as of Mar 2010	$1.01 \pm 0.01 \times 10^7$ n/s

3.4   G-M Tubes

The G-M tubes used in the silver detectors made by AFRL are the 72519 Thin Walled Beta/Gamma tubes from LND, Inc. The tubes are filled with neon gas, quenched and have a stainless steel wall. These tubes were chosen because the 1B85 Thyrodes manufactured by the Victoreen Instrument Company used by Lanter and Bannerman during their calibration are no longer made. Of the six tubes received from AFRL, four were used in the silver detector. Prior to the PuBe source calibration experiment, the G-M tubes were tested using known beta and gamma sources. An examination of voltage curves, dead time, simultaneous count issues and intrinsic efficiency was accomplished.

3.4.1   Voltage Curves

The G-M tube works best when the voltage is high enough to discharge the entire tube as discussed in Section 2.4.3. The operating voltage was found by creating a voltage curve to determine the location that the count rate plateaus. This was accomplished by measuring counts at different voltages using a ^{90}Sr beta source.

38

Counts were measured using an ORTEC 776 counter/timer in 30 second increments for voltages ranging from 750-1200 V. The counts at each voltage was measured three times and averaged.

3.4.2 Simultaneous Counts

When four G-M tubes were in the silver detector's summed configuration and the voltage output was analyzed by an oscilloscope, higher voltage signals were occasionally noticed. This higher voltage was due to the summed signal of two or more G-M tubes after their signals are processed through the bias-T. An ORTEC multichannel buffer and the GammaVision multichannel analyzer software, which separates signals by the signal strength, was used to distinguish how often these simultaneous counts occurred. Simultaneous signals from multiple G-M tubes are possible, but the probability decreases significantly with the number of tubes registering a pulse at the same time.

The simultaneous counts were measured with a ^{90}Sr beta source and with the PuBe source. For the ^{90}Sr beta source two measurement geometry's were used. The first placed the four tubes directly next to each other. The second spread the tubes out by 4 inches to simulate the 4 inch separation that is observed in the silver detector. The data for the ^{90}Sr source can be found in Appendix A in Section 1.1. Simultaneous counts measured from the PuBe source background was conducted to determine the probability of simultaneous counts for the source and detector configuration of the AFIT research.

3.4.3 Dead Time

The minimum time required for a detection system to register two events as two separate pulses is called the dead time of that system [14]. For a G-M tube, the

dead time is the amount of time it takes the tube to return to neutral after an event. Sources of dead time include an avalanche recovery and electronic system lag time. When pulses are not recorded because the tube is dead, the pulses tend to "pile up" and are not counted. When the counting rate is high, the dead time of the system will cause pile up losses affecting the overall count significantly. In contrast, when the counting rate is low, pile up will not be an issue during the dead time of the system.

The dead time was measured for the G-M tubes separately. The two-source method was used to calculate the dead time which compares the counts from two sources individually with the counts from those sources in combination [14]. The dead time, τ, is

$$\tau = \frac{X(1 - \sqrt{(1 - Z)})}{Y} \tag{33}$$

where

$X = m_1m_2 - m_bm_{12}$

$Y = m_1m_2(m_{12}+m_b)-m_bm_{12}(m_1+m_2)$

$Z = \frac{Y(m_1+m_2-m_{12}-m_b)}{X^2}$

m_1 = observed counts from source one

m_2 = observed counts from source two

m_{12} = observed counts from both sources together

m_b = observed counts from background

To ensure the sources are active enough to cause dead time in the tube, the observed counts from all sources multiplied by the fractional dead time, $m_{12}\tau$, should be at least 20%.

Various combinations of two sources were tried, however, the fractional dead time of these measurements was never close to 20%. Therefore, a combination of three sources was found to fulfill the fractional dead time requirement. The sources chosen were a ^{60}Co source, a ^{90}Sr source and a ^{57}Co source. The ^{57}Co source was the first source to be placed. It was placed beneath the G-M tube, approximately 12 mm, and a 30 second measurement was taken. The ^{60}Co and ^{90}Sr were added together directly on the top of the G-M tube and a second 30 second measurement was taken, as shown in Figure 18. Finally, the ^{57}Co source was removed from below the GM tube and a
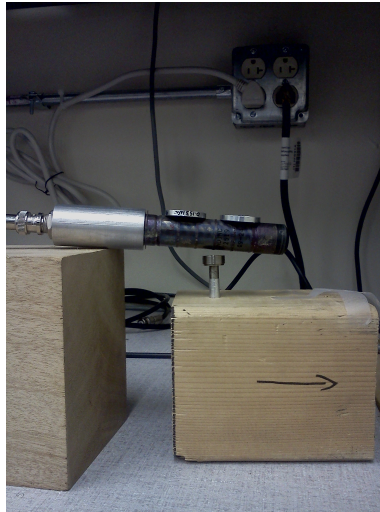
Figure 18. The orientation of the sources and the G-M tube during a measurement when all three sources were present.

final 30 second measurement was taken. This procedure was accomplished three times for each tube to gain statistical integrity. Three 30 second background measurements were also recorded.

3.4.4 Efficiency

The intrinsic efficiency of a detector is the ratio of the amount of radiation detected by the detector to the amount that was incident on the detector. The G-M tubes in the silver detector measure the number of beta or gamma particles that cause a pulse to the electronics. The source was placed 11 mm below the center of the G-M tube for tubes 1, 3, and 4 and 13 mm below tube 2. Counts were taken for 300 seconds. This was repeated three times for each tube and the counts were averaged. The intrinsic efficiency was determined by

$$\epsilon_{int} = \frac{C}{S}\frac{4\pi}{\Omega} \tag{34}$$

where C is the observed count rate accounting for background, S is the source activity, and Ω is the solid angle (in steradians) subtended by the detector at the source position [14].
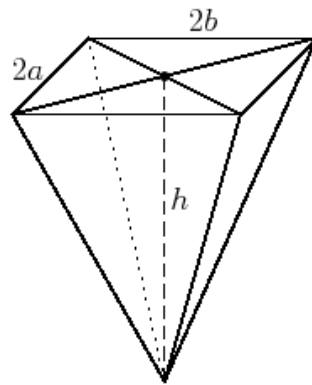
Figure 19. To determine the solid angle subtended by the G-M tube and the source. The G-M tube is represented by the 2a × 2b plane and the beta source is represented as a point source, a distance h below the bottom of the tube. [19]

The solid angle subtended by the detector was determined using a right rectan-

gular pyramid point source approximation shown in Equation 35

$$\Omega = 4 \arcsin \frac{ab}{\sqrt{(a^2 + h^2)(b^2 + h^2)}} \tag{35}$$

where a, b and h are defined in Figure 19 [19]. The solid angle subtended by the tubes positioned 11 mm away is 2.6 steradians and the tube that was 13 mm away is 2.2 steradians.

3.5   Distance Calibration

To create a calibration curve for the silver detectors a PuBe source was used to irradiate the silver detector at various distances away from the source. The silver detector was placed on a table with wheels and the table was positioned at distances ranging 12" to 60" away from the source as shown in Figure 20. The 2.25" and 6" measurements were made after the silver detector was placed on a plank held with weights mounted to the table. The PuBe source was stored inside a paraffin filled metal container. The source was placed inside a smaller aluminum holder with a wire handle that allowed the source to be moved out of the storage container with ease. A carabiner was attached to the holder to raise and lower the source using a pulley system made of parachute cord. The cord pulley system was designed to minimize spin and swing of the holder when the source was raised or lowered. The source had to be raised slowly and steadily to minimize the spin and swing.

The PuBe source differs from the FRCHX experiment and the Cockcroft-Walton accelerator in three ways. First, it does not emit the same neutron spectrum as a typical D-D reaction as discussed in Section 3.2. Second, the PuBe source is continuously emitting neutrons. Third, if the PuBe source is pulsed to create a burst of neutrons, the timing between a pulse from the FRCHX, the accelerator, and the

43

PuBe pulse would all be different. In order to properly create a pulse using the PuBe source, the detector and source had to be in the same room at all times. Three 4" thick borated polyethylene blocks were place around the paraffin filled container holding the PuBe source as shown in Figure 20. The background counts were cut in half when the borated polyethylene was used, however, they were still high overall. Therefore, to compensate for the high background, the silver detector was allowed to reach background saturation prior to any measurements. The PuBe source was pulsed by manually raising the source as shown in Figure 21. To follow ALARA standards for exposure, the operator stood behind a cinderblock wall when the source was raised. A funnel made of a poster board was place inside the PuBe paraffin container to guide the source when lowered to ensure it was placed inside the container without the operator standing in the immediate vicinity.
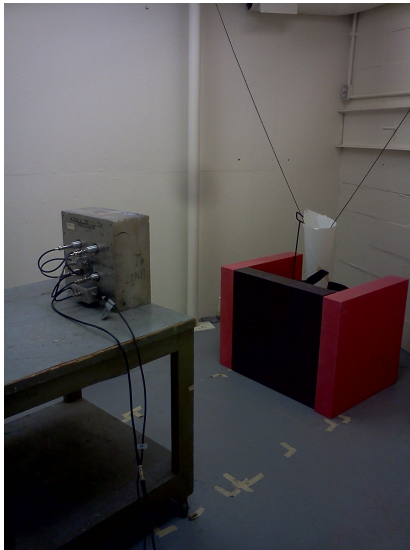
Figure 20. PuBe source in the background configuration. The source is in the paraffin filled container and is surrounded on three sides by 2' × 2' × 4" borated polyethylene.

Figure 21. Picture of the source at the full height of the pulse. The funnel was made of poster board and was used to guide the source back into the container.

When doing this type of calibration experiment, it is important to know the

neutron yield of the source, therefore, the pulse time was recorded. The average time to raise or lower the source was 3.17 ± 0.01 seconds. The source was held in the raised position for an average of 10.29 ± 0.01 seconds. It took an average of 1.78 ± 0.01 seconds to start the measurement after the source was lowered into the container. The burst of neutrons from the pulse was considered to start and stop when the source broke the threshold of the storage container. The threshold of the storage container was half-way between the bottom of the container to the peak height position. Therefore, the overall pulse was approximately 13.46 ± 0.01 seconds. To correct for the delay between burst of neutrons and measurement, the activation foil analysis technique described in Section 2.4 was used. Measurements were performed at 2.25", 6", 12", 24", 36", 48" and 60". At least three measurements at each distance were performed and the results were averaged.

The pulse time that created a burst of neutrons from the FRCHX device, accelerator, and PuBe source range from 10^{-7} to 10^{-6} seconds, 10^{-1} to 10^{0} seconds, and 10^{0} to 10^{1} seconds, respectively. The timing differences are a concern because some of the silver will decay during the burst of neutrons. Therefore, some decays will be missed when the detector begins to measure the G-M tube signals.

The half-life of a material is defined as the time it takes for half of the radioactive atoms in a given sample to disintegrate [6]. The half-lives of the two natural silver isotopes are 24.6 seconds and 2.4 minutes. All three neutron generator systems create a burst of neutrons that is shorter than the 2.4 minute half life by at least an order of magnitude. Because the PuBe source was manually pulsed, it was not physically possible to create a burst of neutrons that occurred less than in the seconds range. To minimize the loss of counts during the time of the burst, the burst time was kept below 24.6 seconds.

The silver foil decays proportionally to $e^{-\lambda t}$, where λ is the effective decay constant

of the two isotopes found in Appendix B. The percentage of radioactive atoms that disintegrates during the burst of neutrons can be determined by

$$\%lost = (1 - e^{\lambda t_{\text{pulse}}}) \times 100\%. \tag{36}$$

A negligible 0.002% of radioactive atoms disintegrate during the FRCHX pulse. This calculation assumed the FRCXH pulse time plus operator reaction time to start the measurement was 10^{-3} seconds. For the accelerator using a 1 second burst of neutrons, a maximum of 2.0 % of the radioactive atoms disintegrate. For the PuBe source using an average pulse time of 13 seconds, a maximum of 24% of the radioactive atoms disintegrate. These percentages are labeled as maximums because the foil is irradiated continuously. If the continuous pulse is described as discrete wavefronts hitting the silver foils and activating a certain number of neutrons for each wavefront, the first wavefront activated atoms will have 24% of those disintegrate, however, the last wavefront will have a negligible amount disintegrate. Therefore, these percentages do not represent the total amount lost, simply the maximum amount lost from a single wavefront. The pulse length for the PuBe source experiment was chosen specifically so that less than 25% of the first wavefront activated atoms would have decayed.

The distances of 2.25" - 12" were influenced by the extreme change in the PuBe source flux while it was being raised and lowered as part of the pulse. The solid angle changes on the order of 4.7 steradians as the detector was raised or lowered from top to bottom of pulse. This extreme and rapid change in solid angle caused a change in the number of neutrons incident on the detector. The calculations for C_t assumed the pulse began as soon as the source crossed the threshold of the storage container. This threshold was half way between the bottom of the container and the top of the container. However, when the detector was closer to the source, a change of a few inches essentially created another burst of neutrons. This research did not take

into account the change in solid angle during the raising and lowering of the source because at the distance of interest the solid angle only changed by 0.071 steradians.

IV. Results and Analysis

4.1 GM Tubes

4.1.1 Voltage Curve

The voltage curve experiment was set up as discussed in Section 3.4.1. Figure 22 shows the voltage curve for the four G-M tubes used in this research. The 950 V bias
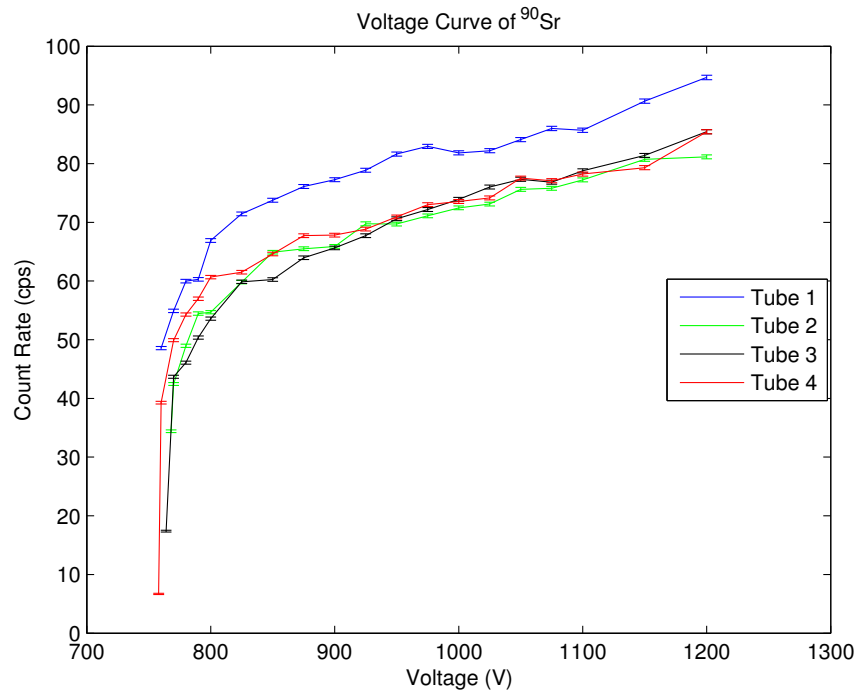
Figure 22. A voltage curve determining the plateau region for each tube using a ^{90}Sr source

used by AFRL is in the plateau region for these detectors, therefore, the remainder of this research will use 950 V bias to be consistent with the bias used by AFRL.

4.1.2 Simultaneous Counts

Figure 23 shows a semi log GammaVision output plot from a 7000 second mea-
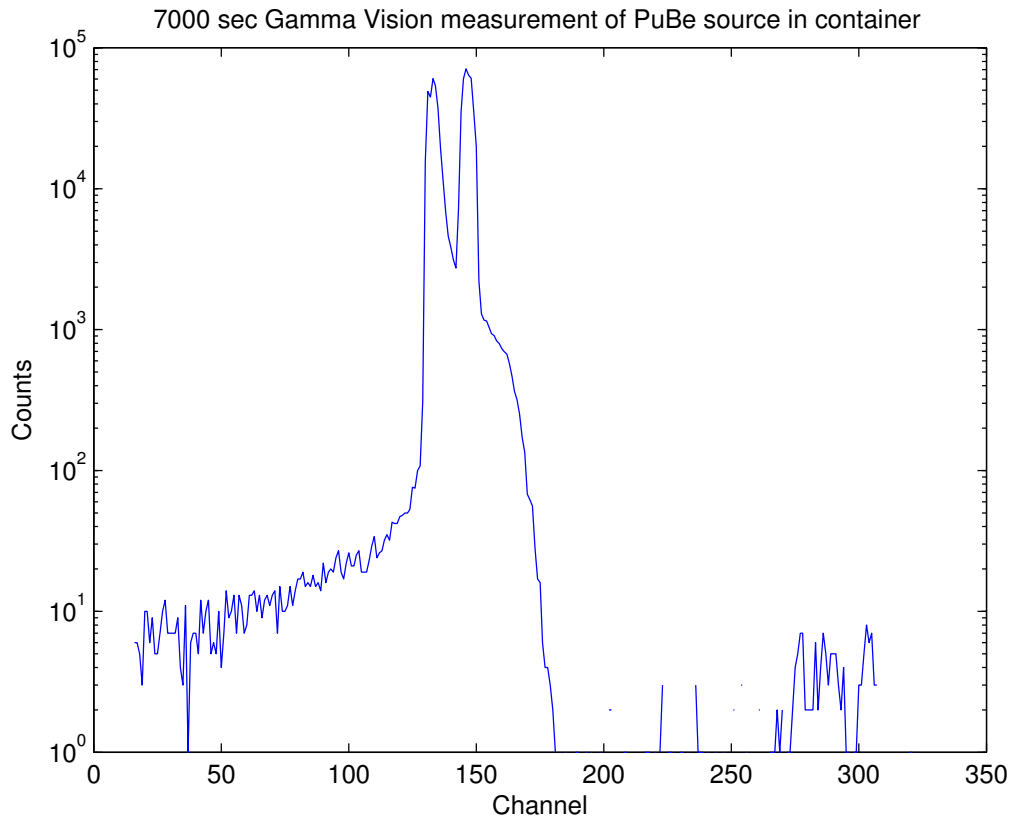
Figure 23. Results of a 7000 second count of the background when the PuBe source was in the room. The peak near channel 150 indicates signals from one tube. The peaks near channel 300 indicates simultaneous signals from two tubes. No simultaneous signals from 3 or 4 tubes were present.

Table 3. Dead time and the fractional dead time for tubes 1-4. The sources are considered active enough to cause dead time in the tube when the fractional dead time is above 20%.

Tube	τ (ms)	$m_{12}\tau$ (20%)
Tube 1	0.10 ± 0.07	22.6
Tube 2	0.11 ± 0.04	22.8
Tube 3	0.11 ± 0.1	21.4
Tube 4	0.10 ± 0.06	20.8
Avg Tube	0.11 ± 0.02	21.9

surement of the PuBe source background. The signals measured from a single G-M tube are shown near channel 150. The signals measured from two G-M tubes simultaneously are shown near channel 300. No simultaneous pulses were measured from three or four G-M tubes due to the low probability of occurrence. Figure 22 shows a difference in counts for each of the four tube operating at the same voltage, therefore, the split peak is probably due to a summing of single tube counts from each of the four G-M tubes. The ratio of pulses measured from two tubes to those from one tube for the 7000 second measurement is $\frac{181}{685389} = 0.026\%$.

The PuBe source was pulsed creating a burst of neutrons and a measurement for a 60 second interval was taken, as described in Section 3.5. It was found that no signals from multiple tubes were present as shown in Figure 24. A correction factor for simultaneous counts from multiple G-M tubes will not be included in this research due to the low probability of occurrence.

4.1.3 Dead Time

Table 3 shows the dead time, τ for the G-M tubes 1 thru 4 which were the tubes used in the silver detector during the PuBe distance experiment. The fractional dead time, $m_{12}\tau$, of each of the four tubes was greater than 20%. This indicates that there

50

60 sec Gamma Vision measurement of PuBe source after a pulse
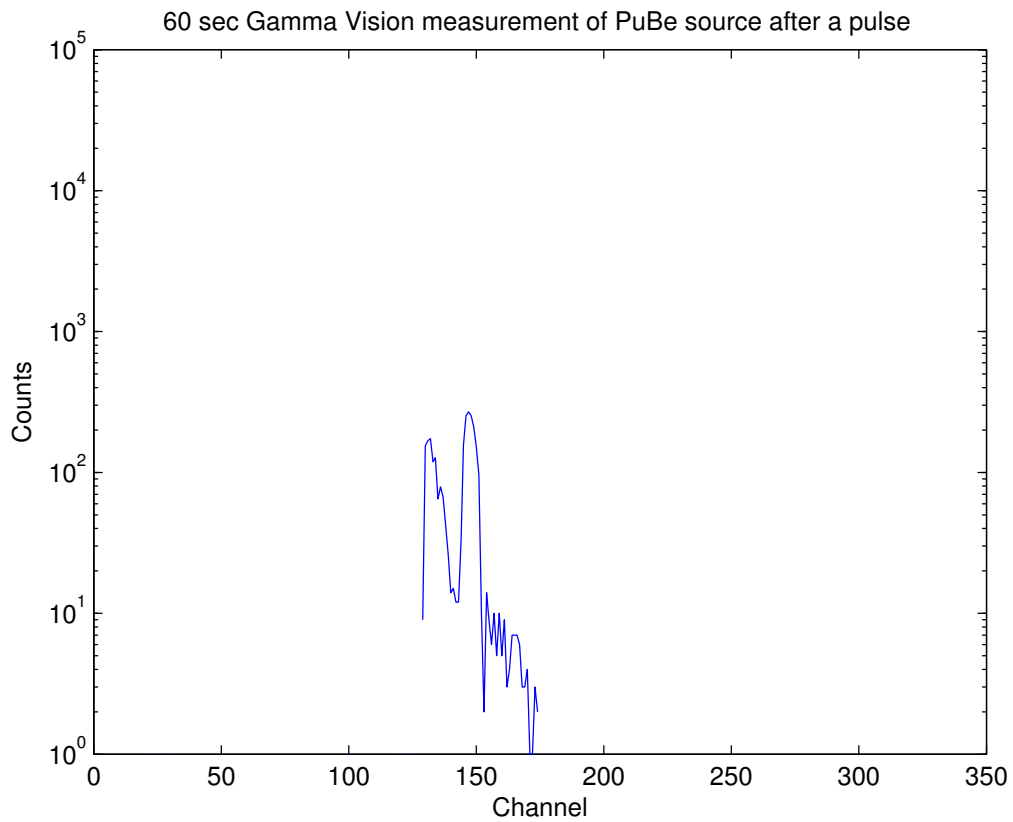
Figure 24. Results of a 60 second count after the PuBe source is pulsed. The peak near channel 150 indicates signals from one tube. No simultaneous signals from 2, 3 or 4 tubes were present.

www.manaraa.com

Table 4. Ratio of actual events to measured counts. Dead time is considered negligible in this research because the distance of most concern, 48", the dead time correction causes less than a 1% increase.

Distance (inches)	Actual Events / Measured Counts
2.25	1.047
6	1.024
12	1.015
24	1.008
36	1.006
48	1.005
60	1.004

is confidence in the measurement because the activity was strong enough to create dead time in the G-M tube. The average dead time for tubes 1-4 individually is 110 +/- 2 μs. The manufacture's minimum dead time listed for these tubes is 100 μs, which matches the findings of this research well [1].

To determine if a dead time adjustment was necessary, the average background rate was subtracted from the count rate to determine the recorded count rate obtained from the PuBe calibration experiment. The recorded count rate was adjusted for dead time using a non-paralyzable model. By using

$$n = \frac{m}{1 - m\tau} \tag{37}$$

where m is the recorded count rate and τ is the dead time, the true interaction rate, n, was determined [14]. The true interaction rate was multiplied by the time interval that the counts were measured to determine the number of actual events for that measurement. Using the dead time average of tubes 1-4 (110 μs) the ratio of dead time actual events to measured counts is shown in Table 4.

The counts measured at 2.25", 6" and 12" distances are increased by less than 5%

52

Table 5. **The intrinsic efficiency found using Equation 34 for tubes 1-4.**

Tube	Efficiency
Tube 1	2.3 ± 0.1e-4
Tube 2	3.4 ± 0.2e-4
Tube 3	2.6 ± 0.2e-4
Tube 4	3.3 ± 0.2e-4
Average	2.9 ± 0.4e-4

due to the dead time adjustment. The counts measured at 24", 36", 48", and 60" are all increased by less than 1%. The 48" distance of interest shows a 0.05% increase. Therefore, the dead time correction will be ignored due to low percentage of increase from the dead time adjustment, particularly at the distance of interest.

4.1.4 Intrinsic Efficiency

The intrinsic efficiency experiment used a ^{90}Sr source and was described in Section 3.4.4. The intrinsic efficiency results for tubes 1-4 are shown in Table 5. The average intrinsic efficiency of beta decay detection for tubes 1-4 was found to be 0.029 ± 0.004%.

4.2 PuBe Source Distance Measurement

The number of counts the detector would have measured, within error, had there been no delay between burst of neutrons and measurement can be found by using the Equations 22 and 26. The activity of this silver foil

$$A_0 = \frac{\lambda}{\epsilon} \frac{(C - B)}{e^{\lambda t_0}(e^{-\lambda t_1} - e^{-\lambda(t_1 + t)})}. \tag{38}$$

was used in the counts equation to determine the corrected counts with no delay between burst and measurement

$$C_{Corr} = \frac{\epsilon}{\lambda} A_0 e^{\lambda t_0} (e^{-\lambda t_0} - e^{-\lambda(t_0 + t)}) \tag{39}$$

where

t is measurement time length of 60 seconds,

t_0 is the time at which the burst of neutrons ceases,

t_1 is the time at which the silver detector begins the measurement,

C is the counts measured from t_1 to $(t_1 + t)$,

B is the average background counts,

λ is the effective decay constant shown in Equation 27,

ϵ is the absolute efficiency of the G-M tubes to measure silver foil decays,

A_0 is the activity of the silver foil at t_0,

C_{Corr} is the corrected counts during the time interval from t_0 to $(t_0 + t)$

By substituting Equation 38 into Equation 39 the resulting equation is

$$C_{Corr} = (C - B)e^{\lambda(t_1 - t_0)}. \tag{40}$$

The silver detector was used to measure counts from a PuBe source at distances ranging 2.25" to 60" during the times t_1 and $(t_1 + 60s)$. Figure 25 shows the corrected counts that the silver detector would have measured at the time t_0, for each distance using Equation 40. The line of best fit for this data was determined using the power law

$$C_{Corr} = 63000D^{-1.13} \tag{41}$$

54
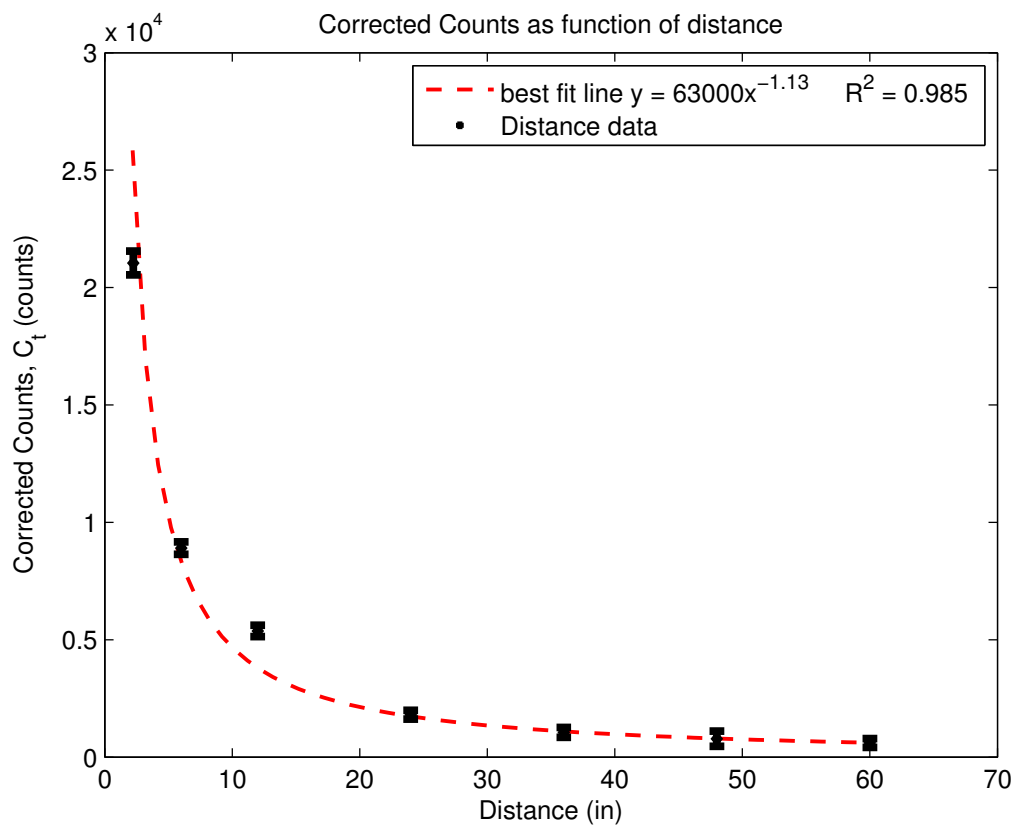
Figure 25. The corrected counts that the G-M tubes would detect at the time the source was removed

where D is the distance in inches between source and detector. Dead time, simultaneous counts, and different types of gamma radiation have all been analyzed and considered within acceptable error to discount, particularly at the 48" distance of interest. Therefore, C_{Corr} was used as the true count, C_t, discussed in Section 3.1.

4.3   Calibration Factor Comparison

The calibration factors used by both Lanter and Bannerman and AFRL relate the neutron yield, N, to the corrected count rate, C_t obtained from taking a 60 second count after burst of neutrons. The neutron activity for the PuBe source used was $1.01 \pm 0.01 \times 10^7$ n/s, and the average pulse time was determined to be 13.46 ± 0.01 s. Therefore the average neutron yield at all energies, N, for a pulse during this experiment was $1.36 \pm 0.01 \times 10^8$ neutrons. Equation 42 was used to determine the calibration factor, F_{PuBe} using N and C_t.

$$F_{PuBe} = \frac{N}{C_t} \tag{42}$$

The source neutron yield is different for each data point due to the varying time it took the source to be raised, held and lowered. Figure 26 shows the average calibration factor values with error, along with the propagated calibration factor equations of Lanter and Bannerman and AFRL. Lanter and Bannerman's results for their data is also shown in red. To better compare the three calibration factors, an equation of the same form was found for the PuBe source. This was accomplished using Mathematica's [25] least-squares FindFit function giving

$$F_{PuBe} = 55.6(9.0 + D)^2 \tag{43}$$

where D is the distance from the source to the moderator face in inches. An alternate

56
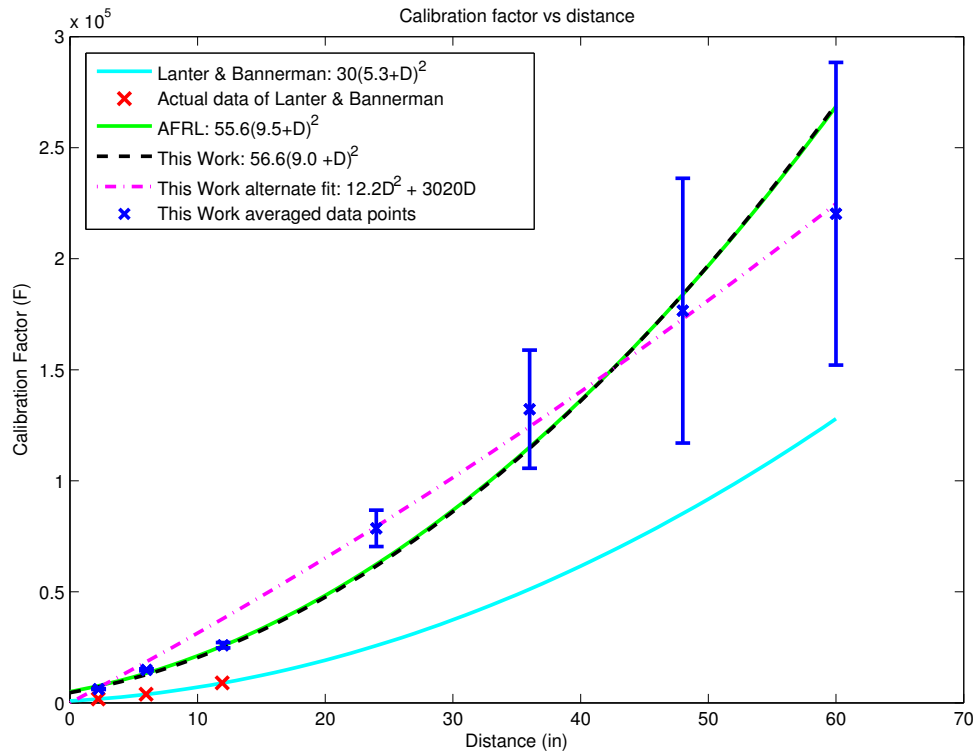
Figure 26. The average calibration factor, F_{PuBe}, with errorbars, for each distance. In addition the calibration factors of Lanter and Bannerman as well as AFRL are shown for comparison.

57

fit of the data points for F_{PuBe} was determined by comparing various least squares fits using the average values at each distance and choosing the line with the best R^2 value. The equation with the best least squares fit with an R^2 value of 0.994 was found to be

$$F_{PuBe} = 12.2D^2 + 3020D \qquad (44)$$

where D is the distance in inches from the source to the face of the moderator of the detector.

It is expected that the Lanter and Bannerman calibration would be different than the calibration done using the PuBe source because the G-M tubes were made of different materials. The calibration factor found in the AFRL research forced a fit using data determined by the Lanter and Bannerman calibration equation. Figure 26 shows that the calibration factor determine by this research very closely matches what AFRL was using for distances below 12". Above 36", the AFRL and AFIT calibration curves are the same within statistical uncertainty. The error increased at greater distances due to the diminishing distinguishability of counts from background. For the distance of interest, 48", the calibration curves from the AFRL calibration and this work are essentially the same within statistical uncertainty. Therefore, neither calibration factor found by this research changed the large order of magnitude difference between experiment and simulation of the FRCHX device.

V. Conclusion

5.1 Conclusion

During the initial design of the FRCHX device, magnetohydrodynamic simulations using MACH2 done by Los Alamos National Laboratory predicted a neutron yield on the order of 10^{12} neutrons [26]. However, AFRL has only measured 10^7-10^8 neutrons from the FRCHX. The disagreement between the experimental and simulated neutron yield implies the simulation, the neutron detection system, and/or the MTF device are not well understood.

The Geiger Müller tubes used in the silver detector during the PuBe source calibration experiment were first analyzed using known beta and gamma sources. The 950 V bias used by AFRL was verified to be on the plateau region of the voltage curve. Simultaneous counts from multiple G-M tubes were determined to be negligible. Only 0.026% of the counts from a 7000 second measurement were from a two tube simultaneous signal. Simultaneous signals for three and four tubes were not detected in the measurements conducted. The average dead time for an individual tube was 110 ± 2 μs. The number of counts that were obtained in the PuBe source calibration were low enough, that the dead time correction was unnecessary. A known ^{90}Sr beta source was used to determine the intrinsic efficiency of the G-M tubes to detect betas. The average tube intrinsic efficiency was found to be $0.029 \pm 0.004\%$.

This research determined that the silver detectors being used during AFRL's FRCHX experiment were properly calibrated at close distances. Above 36", to include the distance of interest at 48", the AFRL and AFIT calibration curves were the same within statistical uncertainty. Therefore the new calibration factor found does not change the large order of magnitude difference between experiment and simulation

59

of the FRCHX device. More research into the simulation and experiment will be necessary.

5.2 Future Recommendations

There are some areas of this research that could be improved. The thermal cross section was used to determine the effective decay constant. However, there are some resonance regions of the silver isotopes that are quite large as seen in Figure 17 and should be considered. The decay of the metastable states of ^{108}Ag and ^{110}Ag have long half-lives that were ignored during this research. The stainless steel of the LND, Inc G-M tube walls are made of many elements that could be activated by exposure to a neutron flux which could affect the counts due to differing half-lives. A study into these three areas should be accomplished to improved the PuBe source calibration curve.

Various MCNP simulations could be run to supplement this work. Two simulations of the PuBe calibration experiment should be executed, one with the cinderblock walls of the room and one without. This will determine if the scattering off the wall has an effect on the measurements. Of specific interest are the 48" and 60" distances, since the walls get closer to the detector as the detector is moved farther away from the source.

An MCNP model of the FRCHX experiment and testing area environment should be built. This could be used to determine the neutron flux in the silver foil for the D-D fusion spectrum in the FRCHX environment. This spectrum should be compared with the neutron flux in the silver foil of the PuBe source simulation that included the cinderblock walls. This will provide a more robust comparison of the PuBe source activated detector and environment to the FRCHX D-D fusion source activated detector and environment. A model of the entire FRCHX testing area

60

using a tool such as Scale 6.1 would be useful to determine optimal placement of the detectors around the FRCHX device based on dose information. Scale 6.1 is a modeling and simulation program that focuses on safety and shielding.

More MACH2 simulations of the FRCHX would provide the data needed to determine trends and averages of neutron yield. By improving the simulation, a better understanding to the overall FRCHX device should follow. Also, an analysis of the spectrum of neutrons emitted from the FRCHX fusion would be useful. Spectral information would enhance the MCNP simulations by improving the accuracy of the source term in simulations. Spectral information would also provide much insight into the D-D fusion reaction of the FRCHX device.

Appendix A.   Additional Measurements

There were six G-M tubes that AFRL sent to AFIT to be used in the silver detector. Only four were needed in the detector, but the voltage curve, dead time and efficiency measurements were accomplished for all six tubes. The following tables and figures show the data for all six tubes.

1.1   Voltage
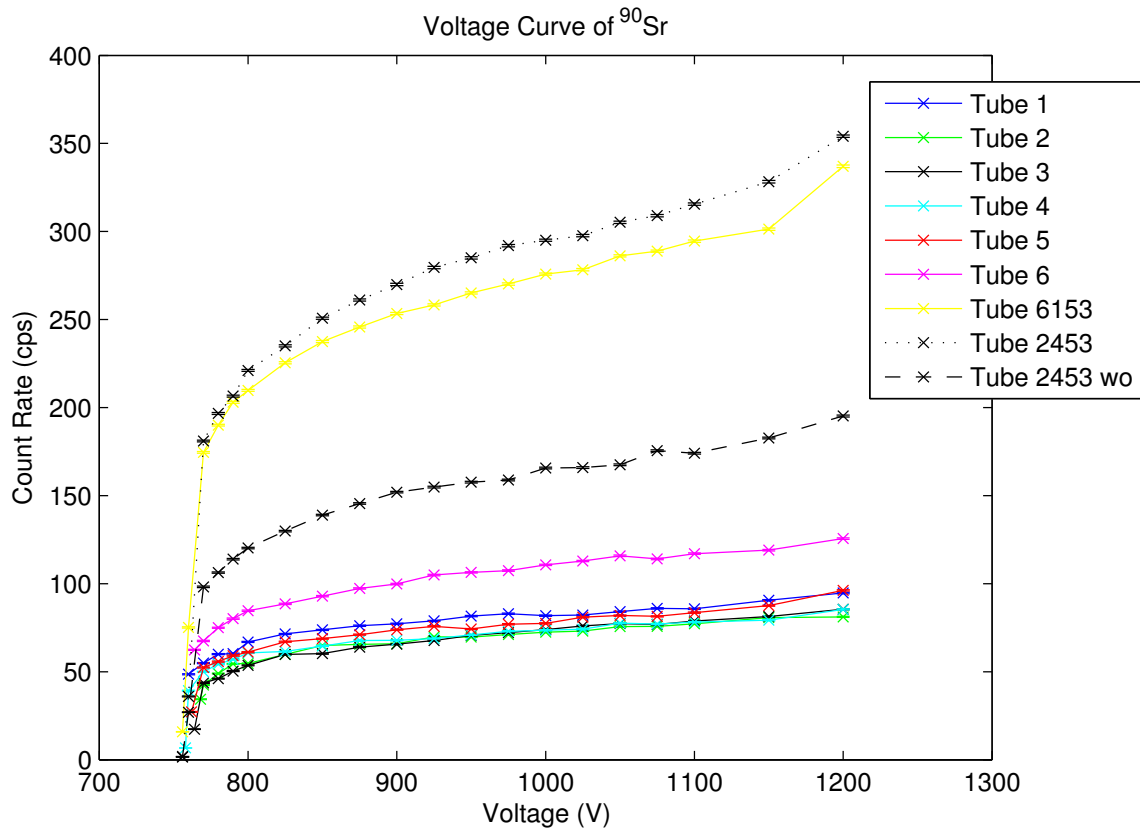
Figure 27. Voltage curve using a ^{90}Sr source for all measurements taken.

Figure 27 shows the voltage curves for each of the tubes sent by AFRL. Tube 6153 and Tube 2453 denote the measurement when all four tubes 6, 1, 5 and 3 or tubes 2, 4,

5 and 3 were connected together. The measurements were accomplished using a disk source while it was in its storage container with the top flipped open. To compare cps without the container present, Tubes 2453 wo is shown. This means that the container was causing scattering to occur. The container did not change the overall result, which was to ensure the tubes were being operated properly at 950 V. The figure shows that for all tubes, 950 V is in the plateau region. Three measurements at each voltage were taken and averaged together. Error bars are shown on this graph, however, they are too small to be detected.

1.2 Simultaneous Counts

Prior to using GammaVision on the PuBe source to detect simultaneous counts, a different GammaVision test was accomplished using the Sr-90 source placed below the four tubes. Two measurement geometries were used. The first placed the four tubes directly next to each other. The second spread the tubes out by 4 inches to simulate the 4 inch separation that is observed in the silver detector. When the four tubes, tubes 2, 4, 5 and 3 were directly next to each other, GammaVision and the counter/timer were used to verify that GammaVision was collecting the same number of counts the counter/timer was reporting. There were 19785 counts measured by the counter/timer during a 60 second and GammaVision reported a total of 19785 counts. The one event channel area was very spread out, but 19445 counts are considered in the one event channel area, 337 counts were in the two event channel area and 3 counts were in the three event channel area. There were no counts in the 4 event channel area. The main peak of the one event channel area showed 19176 counts. The remaining 269 counts of the 19445 were in channels below the main peak. Thus, GammaVision was counting the same number of counts as the counter/timer.

Figure 28 shows four plots where the right plots are zoomed versions of the cor-

63

responding left plots. The top plots are from a two hour run and the bottom plots are from a 60 second run. For both runs the G-M tubes are positioned 4" apart horizontally. The top-right zoomed plot shows counts in the one, two and three event channel areas. One event corresponds to channels near 150, two events are shown near channel 300 and three events are shown near channel 450. There were no counts detected in the 4 event area, which can be deduced to be near channel 600. The bottom graphs of the Gamma Vision output had the counter/timer running simultaneously. The counter/timer measured 1047 counts, Gamma Vision's main peak measured 1043 counts. There was 1 count below the main peak and 3 counts are in the two event region, therefore the total number of counts measured by Gamma Vision is the same as the counter/timer.
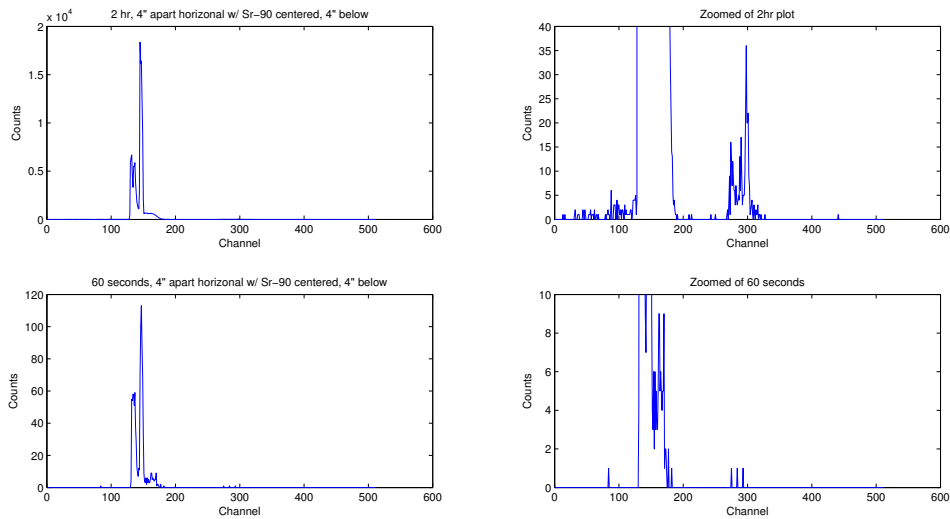
Figure 28. Gamma Vision comparison of a 2hr count and a 60 second count. Areas surrounding 150, 300, and 450 represent one event, two events and three events respectively.

Table 6. Dead time data. All data is in the form of counts. Measurements were taken in 30 second increments.

	Tube 1	Tube 2	Tube 3	Tube 4	Tube 5	Tube 6
^{57}Co	35231	36731	27683	32569	31401	25513
	35257	36574	27710	32184	31438	25336
	35853	36455	27833	32431	31494	25364
^{57}Co^{60}Co^{90}Sr	65351	64711	57366	61861	60248	53760
	65151	64887	57083	61412	59930	53518
	65458	65057	56534	61466	59922	53740
^{60}Co^{90}Sr	38324	36654	36287	36316	35915	34349
	38145	36572	35518	36389	35855	34403
	38165	36776	36081	36266	35752	34249
Background	16	15	10	15	16	19
	21	11	16	14	15	15
	13	23	16	14	10	22

1.3 Dead Time

Dead time was also measured for all six tubes. The dead time for all tubes was calculated the same way as described in Section 4.1.3. The data for all tubes is presented in Table 6. Results of all dead time measurements are shown in Table 7. The ratio of the non-paralizable dead-time correction on PuBe counts for different distances to the original counts measured for all six tubes received from AFRL is shown in Table 8. It was determined that at the 48" distance of interest the dead time was less than 1% and therefore could be ignored.

65

Table 7. The deadtime measurements for all six tubes received from AFRL. Measurements were done the same way as described in Section 4.1.3

Tube	τ (ms)	$m_{12}\tau$
Tube 1	0.10 ± 0.07	22.6
Tube 2	0.11 ± 0.04	22.8
Tube 3	0.11 ± 0.1	21.4
Tube 4	0.10 ± 0.06	20.8
Tube 5	0.11 ± 0.04	21.6
Tube 6	0.12 ± 0.04	20.8

Table 8. The ratio of the non-paralizable dead-time correction on PuBe counts for different distances to the original counts measured for all six tubes received from AFRL

Distance (inches)	Averaged individual tubes C_t/C
2.25	1.047
6	1.024
12	1.015
24	1.008
36	1.006
48	1.005
60	1.004

1.4 Efficiency

Table 9 shows the intrinsic efficiency for all six tubes. The average for all six tubes is the same as that for four tubes, 0.029 ± 0.004 %. A ^{90}Sr source was used to determine the intrinsic efficiency for beta detection by the G-M tubes.

Table 9. The efficiency found for all six of the tubes received from AFRL.

Tube	Efficiency
Tube 1	2.3 ± 0.1 e-4
Tube 2	3.4 ± 0.2 e-4
Tube 3	2.6 ± 0.2 e-4
Tube 4	3.3 ± 0.2 e-4
Tube 5	2.9 ± 0.2 e-4
Tube 6	2.9 ± 0.2 e-4
Avg 1-6	2.9 ± 0.4 e-4

1.5 Saturation

Counts were taken in various intervals from 15 seconds to 2 minutes for 1 hour. The detector reached saturation to the background radiation from having the PuBe source in the room, represented by the first data point. During the hour the PuBe source was held in the up position and allowed to reach a saturated steady state, returned to the container and allowed to return to background, and raised again. During data analysis it was noticed that between the two source exposures the detector did not reach the true starting background even though the count rate seemed to be steady during the experiment. Therefore, the two peaks of Figure 29 can not be directly compared. This information could be useful if a background measurement of the PuBe source without the silver foil surrounding the G-M tubes was accomplished. This would

67

allow determination of the number of counts that are actually from neutrons when the foil is saturated.
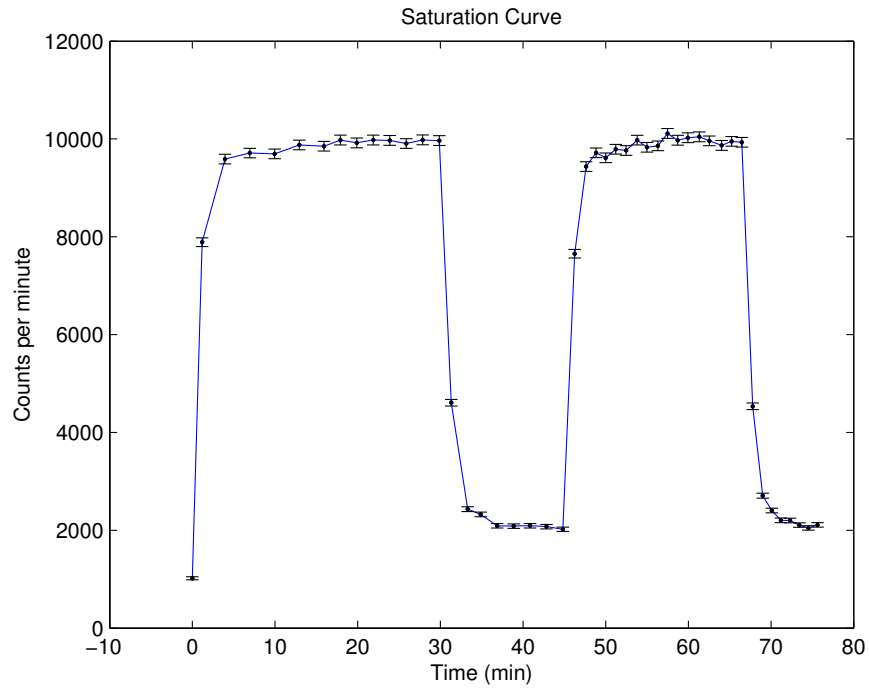
Figure 29. Saturation curve using the PuBe source.

Appendix B. Data and Calculations

2.1 Weighted Decay Constant

Determining the weight percent of isotopes ^{108}Ag and ^{110}Ag for the weighted decay constant described in Section 2.4 is shown in Equations 45 thru Equations 48. The ^{107}Ag isotope is 51.8% abundant and has a thermal neutron cross section of 37 $\pm$ 2 barns, and the ^{109}Ag isotope is 48.2% abundant and has a thermal neutron cross section of 89 $\pm$ 4 barns [27, 21]. Equation 49 is the resultant weighted decay constant where $\lambda_{^{108}\text{Ag}}$ is the decay constant for ^{108}Ag and $\lambda_{^{110}\text{Ag}}$ is the decay constant for ^{110}Ag.

$$\frac{51.8}{100} \left(\frac{37\text{b}}{89\text{b} + 37\text{b}} \right) = 0.152 \tag{45}$$

$$\frac{48.2}{100} \left(\frac{89\text{b}}{89\text{b} + 37\text{b}} \right) = 0.340 \tag{46}$$

$$\frac{0.152}{0.152 + 0.340} = 0.31 \tag{47}$$

$$\frac{0.340}{0.152 + 0.340} = 0.69 \tag{48}$$

$$\lambda = 0.31\, \lambda_{^{108}\text{Ag}} + 0.69\, \lambda_{^{110}\text{Ag}} \tag{49}$$

2.2 PuBe Source Distance Experiment

The actual data from the PuBe source distance experiment is shown in Table 10. Each increment of the source exposure was timed including the time it took to raise the source up, the amount of time the source was held at the full height, and the time it took to lower the source back to the bottom of the container. The amount of time between the source placed at the bottom of the container and the sixty second measurement was recorded is indicated in the Start column of the table. The neutron burst time is considered to be time when the source passes the container threshold

69

on the way up and down. This is found by adding together half the time up, the time held, and half the time down.

Table 10. The actual data from the PuBe source distance calibration experiment.

Dist (in)	Up (s)	Held (s)	Down (s)	Start (s)	Pulse (s)	Counts	Avg Bg
2.25	3.02	10.47	2.56	2.07	13.26	26722	5910 ± 220
2.25	2.66	10.09	2.58	1.67	12.71	25856	5910 ± 220
2.25	2.85	10.17	2.38	1.26	12.79	24518	5910 ± 220
6	3.45	10.78	2.68	1.62	13.84	13416	4968 ± 87
6	2.58	10.20	2.17	1.64	12.57	13552	4968 ± 87
6	2.74	10.17	2.78	1.42	12.93	13110	4968 ± 87
12	4.88	9.52	2.97	2.80	13.44	8681	3769 ± 91
12	3.05	10.45	3.55	1.93	13.75	8649	3769 ± 91
12	4.02	10.62	3.47	2.65	14.36	8767	3769 ± 91
24	3.93	10.51	3.48	1.72	14.22	4529	2863 ± 76
24	3.55	10.76	3.49	1.43	14.28	4520	2863 ± 76
24	3.85	9.91	3.88	1.55	13.78	4590	2863 ± 76
36	4.56	10.33	3.82	1.81	14.52	3354	2402 ± 98
36	4.56	10.16	3.65	1.52	14.26	3385	2402 ± 98
36	2.20	10.49	2.33	1.49	12.75	3430	2402 ± 98
48	4.03	10.52	3.10	1.97	14.08	2675	2007 ± 94
48	3.35	10.29	2.81	1.42	13.27	2714	2007 ± 94
48	3.30	10.23	2.96	1.70	13.36	2782	2007 ± 94
48	2.77	9.89	3.89	1.62	13.22	2720	2007 ± 94
48	3.57	10.31	2.53	1.76	13.36	2738	2007 ± 94
60	2.94	10.17	2.26	1.58	13.33	2277	1670 ± 89
60	3.10	10.50	2.51	1.71	13.31	2245	1670 ± 89
60	3.50	10.00	2.41	1.85	12.96	2196	1670 ± 89

70

Appendix C. Equipment

Table 11. A description of the equipment used for this research.

Equipment Description	Manufacturer	Style #
HV Power Supply	Ortec	485
Counter/Timer	Ortec	776
Wires		RG-223/U
Geiger Müller Tubes	LND, Inc	72519
HV Power Supply	Canberra	3106D

Table 12. A description of the sources used for this research.

Source	Serial #	Calibration Date	Inception Activity	Present Activity
Sr-90	363	01 Nov 1981	0.153 mCi	0.072 mCi
Co-60	T-125	15 Sept 2007	10.26 μCi	6.541 μCi
Co-57	T-122	15 Nov 2011		0.115 mCi
PuBe	M-1170	09 Mar 1962	4685 mCi	4678 mCi

Appendix D. Decay Schemes
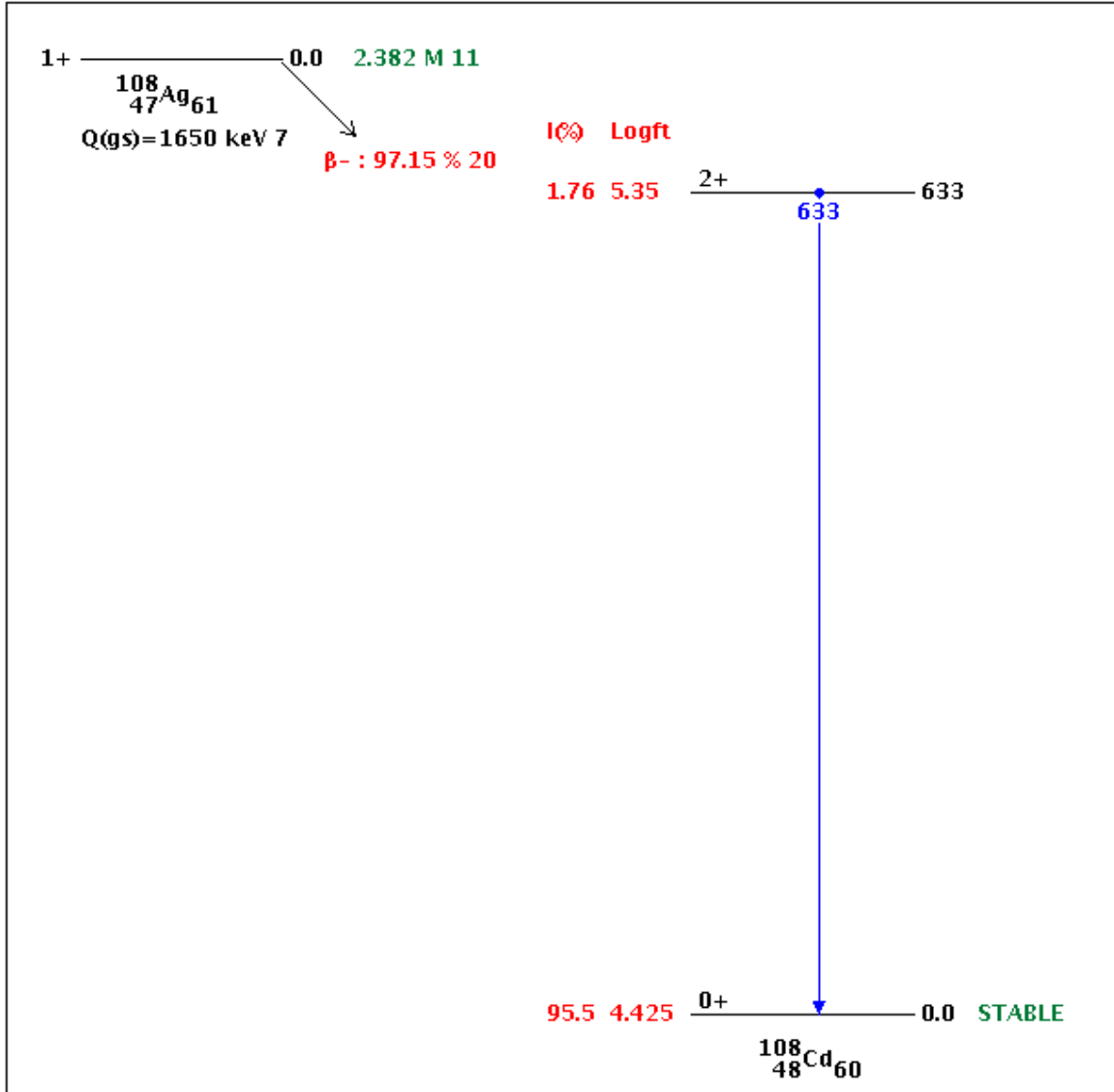

Figure 30. ^{108}Ag beta decay scheme. 95.5% of the time the isotope decays to the ground state of ^{108}Ca, the rest of the time a beta and gamma are emitted. [21]
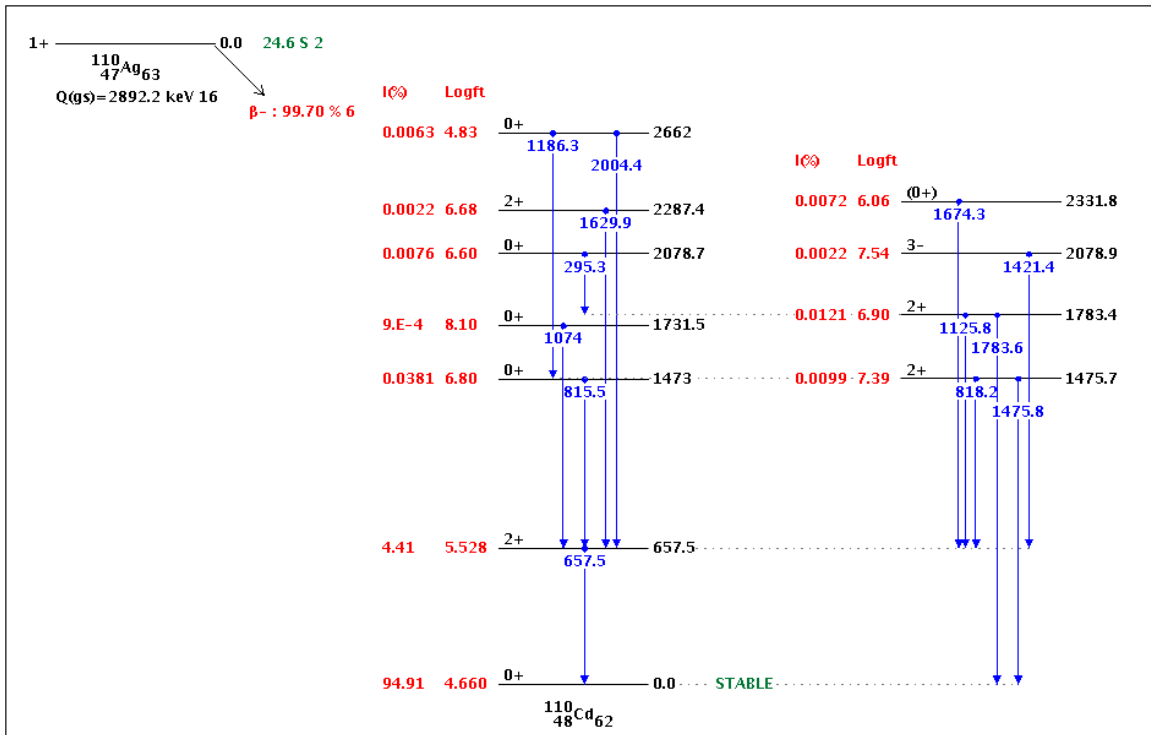
www.manaraa.com

Figure 31. ^{110}Ag beta decay scheme. 94.9% of the time the isotope decays to the ground state of ^{110}Ca, the rest of the time a beta and gamma or multiple gammas are emitted. [**21**]

73

Appendix E. Computer Codes

The code used by AFRL to determine Equation 32 is shown in Figure 32. The FindFit function in Mathematica [25] used the yield, number of counts obtained and distance to determine the correct numbers to go into an equation of the form $A(B+D)^2$ where D is the distance in inches between the source and detector face. Figure 33

```
In[1]:=  Y = {3.1*^7, 3.2*^7, 3.4*^7, 3.3*^7, 3.1*^7}

Out[1]=  {3.1×10⁷, 3.2×10⁷, 3.4×10⁷, 3.3×10⁷, 3.1×10⁷}

In[2]:=  count = {166, 223, 232, 244, 227}

Out[2]=  {166, 223, 232, 244, 227}

In[3]:=  d = {44, 44, 40.6, 40.6, 40.6}

Out[3]=  {44, 44, 40.6, 40.6, 40.6}

In[4]:=  Data = Table[{d[[i]], count[[i]], Y[[i]]}, {i, 5}]

Out[4]=  {{44, 166, 3.1×10⁷}, {44, 223, 3.2×10⁷},
          {40.6, 232, 3.4×10⁷}, {40.6, 244, 3.3×10⁷}, {40.6, 227, 3.1×10⁷}}

In[5]:=  TableForm[Data]

Out[5]//TableForm=
        44     166   3.1×10⁷
        44     223   3.2×10⁷
        40.6   232   3.4×10⁷
        40.6   244   3.3×10⁷
        40.6   227   3.1×10⁷

In[6]:=  FindFit[Data, A (dist + B)² c, {A, B}, {dist, c}]

Out[6]=  {A → 55.5978, B → 9.4636}
```

Figure 32. The Mathematica [25] script used by AFRL to find the calibration factor shown in Equation 32.

shows the Mathematica code using the data from the research done at AFIT. The

74

In[5]:= **TableForm[Data]**

Out[5]//TableForm=

2.25	22 122	1.335×10^8
2.25	21 052	1.2799×10^8
2.25	19 458	1.28744×10^8
6	8916	1.39419×10^8
6	9021	1.2663×10^8
6	8570	1.30205×10^8
12	5312	1.35391×10^8
12	5221	1.38463×10^8
12	5414	1.44656×10^8
24	1775	1.43145×10^8
24	1756	1.438×10^8
24	1841	1.38714×10^8
36	1018	1.46216×10^8
36	1045	1.43649×10^8
36	1079	1.28443×10^8
48	725	1.41735×10^8
48	757	1.33629×10^8
48	834	1.34535×10^8
48	774	1.33125×10^8
48	785	1.34535×10^8
48	638	1.28896×10^8
60	638	1.34233×10^8
60	607	1.33981×10^8
60	556	1.30457×10^8

In[6]:= **FindFit$\left[\text{Data, A (dist + B)}^2 \text{ c, \{A, B\}, \{dist, c\}}\right]$**

Out[6]= $\{A \rightarrow 56.6221, B \rightarrow 8.9822\}$

Figure 33. The Mathematica [25] script used by this research to find the calibration factor shown in Figure 26 under "This work: $56.6(9.0+D)^2$".

75

results were compared with the results found by AFRL and determined to be the same as discussed in the Results and Analysis portion of this paper.

A sample of the MCNP code used in this document is shown below [9]. The geometry for this code is shown in Figure 11. The code is currently set up to run a simulation for a PuBe source, 48" from the front face of the detector. Not all energy bins are shown. The energy bins used were the same as from the bins size used in the silver capture cross-section data from the ENDF database.

```
Flux of neutrons in silver
c GEOMETRY - CELLS
100 3000 -.0008195 -12 +26 -27 imp:n=1 $BR Ne
110 3000 -.0008195 -15 +26 -27 imp:n=1 $BL Ne
120 3000 -.0008195 -18 +26 -27 imp:n=1 $TR Ne
130 3000 -.0008195 -21 +26 -27   imp:n=1 $TL Ne
200 4000 -7.5 -13 +24 -25 (12:-26:27) imp:n=1 $BR Steel
210 4000 -7.5 -16 +24 -25 (15:-26:27) imp:n=1 $BL Steel
220 4000 -7.5 -19 +24 -25 (18:-26:27) imp:n=1 $TR Steel
230 4000 -7.5 -22 +24 -25 (21:-26:27) imp:n=1 $TL Steel
300 5000 -10.5 -14 +24 -25 #200 imp:n=1 $BR Silver
310 5000 -10.5 -17 +24 -25 #210 imp:n=1 $BL Silver
320 5000 -10.5 -20 +24 -25 #220 imp:n=1 $TR Silver
330 5000 -10.5 -23 +24 -25 #230 imp:n=1 $TL Silver
400 2000 -0.94 -11 #300 #310 #320 #330 imp:n=1 $poly box
500 1000 -0.0012 -10 #400 imp:n=1 $Air outside poly
600 0 10 imp:n=0 $boundary


c GEOMETRY - SURFACE
```

```
10 RPP -5.08 172.72 -5.08 35.56 -5.08 35.56 $Outside poly by 2; x= -2in to 62in
11 RPP 0.0 15.48 0.0 30.48 0.0 30.48 $Outer Poly Box of detector
12 C/X 10.16 10.16 0.94488 $Ne bottom right gm
13 C/X 10.16 10.16 0.9525 $3 mil 446 Steel bottom right GM
14 C/X 10.16 10.16 0.9779 $10 mil Silver bottom right GM
15 C/X 20.32 10.16 0.94488 $Ne bottom left gm
16 C/X 20.32 10.16 0.9525 $3 mil 446 Steel bottom left GM
17 C/X 20.32 10.16 0.9779 $10 mil Silver bottom left GM
18 C/X 10.16 20.32 0.94488 $Ne top right GM
19 C/X 10.16 20.32 0.9525 $3 mil 446 Steel top right GM
20 C/X 10.16 20.32 0.9779 $10 mil Silver top right GM
21 C/X 20.32 20.32 0.94488 $Neon left GM
22 C/X 20.32 20.32 0.9525 $3 mil 446 Steel top left GM
23 C/X 20.32 20.32 0.9779 $10 mil Silver top left GM
24 PX 3.1654 $Cut off end of Steel & Silver
25 PX 8.4446 $Cut off other end of Steel & Silver
26 PX 3.173 $Cut off end of Ne
27 PX 8.4192 $Cut off other end of Ne

c OTHER STUFF
nps 1000000000
mode n
print 10 110 170
c MATERIALS
m1000 6012 0.000124 7014 0.755268 $Air
8016 0.231781 18036 0.012827
```

77

```
m2000 1001 0.143711 6012 0.856289 $Polyethylene

m3000 10020 1.0 $Neon

m4000 24052 0.25 26056 0.7198 $446 Stainless Steel

28058 0.0025 6012 0.002

25055 0.015 14028 0.01

15031 0.0004 16032 0.0003

m5000 47107 0.51839 47109 0.48161 $Silver

c m6000 5010 0.01 6000 0.814 $Borated Poly

c 1001 0.136 5011 0.04

c m7000 48000 1.0 $Cadmium

c SOURCE

c Mono-energetic 2.45MeV isotropic, 2.25" from face of poly, centered

c SDEF pos=20.955 15.24 15.24  par=1 erg=2.45

c Mono-energetic 2.45MeV isotropic, 48" from face of poly, centered

c SDEF pos = 137.4 15.24 15.24 par=1 erg = 2.45 $MeV

c Pu-Be Spectrum 2.25" from face of poly, centered

c x,y,z coord, par=1 means neutrons, erg=histogram defined below

c SDEF pos=20.955 15.24 15.24 par=1 erg=d1

c Pu-Be Spectrum 48" from face of poly, centered

c x,y,z coord, par=1 means neutrons, erg=histogram defined below

 SDEF pos=137.4 15.24 15.24 par=1 erg=d1

 SI1 H   4.7e-2 1.4e-1 2.7e-1 4.62e-1 6.38e-1 8.61e-1 1.13 1.42 1.69

         1.96 2.22 2.34 2.52 2.82 3.13 3.48

         3.80 3.99 4.23 4.47 4.66 4.8 4.93 5.09 5.22 5.26 5.44 5.55 5.84

         6.20 6.51 6.89 7.10

         7.40 7.72 7.97 8.15 8.31 8.37 8.47 8.71 9.12 9.46 9.74 9.94 10.11
```

```
          10.27 10.38 10.57 10.69        $Histogram boundaries

  SP1 D  0 1.97 4.01 6.0 7.28 7.64 7.57 7.20 6.77 6.43 6.32 6.50 7.19 8.18

             9.45 10.59 11.01 11.17 11.21 11.15 10.94 10.56

             10.07 9.32 8.68 7.91 7.33 6.77 6.35

             6.14 6.28 6.67 6.85 6.83

             6.71 6.39 5.87 5.28 4.41 3.82 3.19 2.57 2.23 2.28 2.42 2.17 1.73

             1.44 0.95 0.45          $probabilities for each bin

f14:n 300 $Bottom Right Silver

E14 1.000000e-11 1.154357e-11 1.308715e-11 1.617431e-11

        1.926146e-11 2.234862e-11 2.543577e-11 2.852293e-11

        3.469725e-11 4.087156e-11 4.704587e-11 5.322018e-11

        5.939450e-11 7.174312e-11 8.409175e-11 9.644037e-11

        1.087890e-10 1.334862e-10 1.581835e-10 1.828808e-10

        2.075781e-10 2.569726e-10 3.063671e-10 3.557616e-10

        4.051562e-10 5.039452e-10 6.027343e-10 7.015234e-10

        8.003125e-10 9.978907e-10 1.195469e-09 1.393047e-09

        1.590625e-09 1.985781e-09 2.380937e-09 2.776093e-09

        3.171250e-09 3.961562e-09 4.751875e-09 5.542187e-09

        6.332500e-09 7.913125e-09 9.493750e-09 1.107437e-08

        1.265500e-08 1.581625e-08 1.897750e-08 2.213875e-08

        2.530000e-08 2.925407e-08 3.027102e-08 3.320814e-08

        3.524205e-08 4.021307e-08 4.111628e-08 4.518410e-08

        4.902442e-08 5.512615e-08 5.693257e-08 6.484071e-08

        6.506820e-08 7.274886e-08 7.501025e-08 8.495230e-08

        8.856515e-08 1.043814e-07 1.048364e-07 1.201977e-07

        1.247205e-07 1.360140e-07 1.446046e-07 1.518303e-07
```

Bibliography

[1] "LND 72519 Thin wall beta-gamma detector". Internet: http://www.lndinc.com/products/369/, [10 May 2012]. URL http://www.lndinc.com/products/369/.

[2] "Online Plotter for MCNP and ENDF cross section data". Internet: http://atom.kaeri.re.kr/cgi-bin/endfplot.pl, [12 May 2012]. URL http://atom.kaeri.re.kr/cgi-bin/endfplot.pl.

[3] *Handbook on Nuclear Activation Cross-Sections*. Technical Reports Series 156, International Atomic Energy Agency, Vienna, 1974.

[4] "An Introduction to Geiger-Mueller (GM) Detectors". Oak Ridge Associated Universities Internet: http://www.orau.org/ptp/collection/gms/introgms.htm, 1999 [25 Jul 2007]. URL http://www.orau.org/ptp/collection/gms/introgms.htm.

[5] Barnes, Cris W., M. G. Bell, H. W. Hendel, D. L. Jassby, D. Mikkelsen, A. L. Roquemore, S. D. Scott, J. D. Strachan, and M. C. Zarnstorff. "Absolute calibration of neutron detection systems on TFTR and accurate comparison of source strength measurements to transport simulations". *American Institute of Physics*, 61(10), October 1990.

[6] Baum, Edward M., Harold D. Knox, and Thomas R. Miller. *Nuclides and Isotopes: Chart of the Nuclides*. KAPL, Inc, 16 edition, 2002.

[7] Bevins, James. "Calibration of the Graphite Pile at AFIT to account for 241Am ingrowth in Pube Source", March 2009.

[8] Bridgman, Charles J. "Introduction to the Physics of Nuclear Weapons Effects - Unclassified Study Guide". 2010.

[9] Briesmeister, J.F. *MCNP Manual - A General Purpose Monte Carlo N-Particle Transport Code*. Los Alamos National Laboratory Report LA-12625-M, Version 5, Los Alamos National Laboratory, 2003.

[10] Fitzpatric, Richard. "Plasma Physics". Internet: http://farside.ph.utexas.edu/teaching/plasma/380.pdf.

[11] Intrator, T. P., G. A. Wurden, P. E. Sieck, W. J. Waganaar, L. Dorf, M. Kostora, R. J. Cortez, J. H. Degnan, E. L. Ruden, M. Domonkos, P. Adamson, C. Grabowski, D. G. Gale, M. Kostora, W. Sommars, M. Frese, S. Frese, J. F. Camacho, P. Parks, R. E. Siemon, T. Awe, A. G. Lynn, and R. Gribble. "Field Reversed Configuration Translation and the Magnetized Target Fusion Collaboration". *Fusion Energy*, 28:165–169, 2009.

[12] Kashani, M., T. Miyamoto, and Y. Tanimura. "Calibration of silver activation neutron detector". *Iranian Physical Journal*, 2(4):6–10, 2009.

[13] Kirkpatrick, Ronald C. and Irvin R. Lindemuth. "Magnetic Compression/ Magnetized Target Fusion (MAGO/MTF)". *Second Symposium of Current Trends in International Fusion Research*, LA-UR-97-4896. Los Alamos National Laboratory, Washington, DC, March 1997.

[14] Knoll, Glenn F. *Radiation Detection and Measurement.* John Wiley and Sons, Inc, 4 edition, 2010.

[15] Krane, Kenneth S. *Introductory Nuclear Physics.* ISBN 978-0-471-80553-3. John Wiley and Sons, Inc, 1988.

[16] Lanter, Robert J. and Daniel E. Bannerman. *The Silver Counter - a detector for bursts of neutrons.* Technical Report LA-3498-MS, Los Alamos Scientific Laboratory of the University of California, 1996.

[17] Lindemuth, Irvin R. and Richard E. Siemon. "The Basis of Magnetized Target Fusion - A Fusion Primer". *Megagauss Magnetic Field Generation and Related Topics*, 27–36. 2006.

[18] Olsen, Christopher. "Introduction to the Space Environment", November 2009. Naval Postgraduate School.

[19] Pahikkala, J. "Solid Angle of Rectangular Pyramid". Version 13. Internet: http://planetmath.org/?op=getobj;from=objects;id=12198, [May 5, 2012].

[20] Reilly, D. and et. al. *Passivee Nondestructive Assay of Nuclear Materials.* Nuclear Commission Report NUREG/CR-5550 (also LA-UR-90-732), Los Alamos National Laporatory, 1991.

[21] Sonzogni, Alejandro. "Chart of Nuclides". Internet: http://www.nndc.bnl.gov/chart/chartNuc.jsp, [23 May 2012]. URL http://www.nndc.bnl.gov/chart/chartNuc.jsp.

[22] Stewart, Leona. "Neutron Spectrum and Absolute Yield of a Plutonium-Beryllium Source". *Physical Review*, 98(3):740–743, May 1955.

[23] W.B.Wilson, R. T. Perry, W. S. Charlton, T. A. Parish, and E. F. Shores. *Sources-4C: a code for calculating (alpha,n) spontaneous fission and delayed neutron sources and spectra.* Technical Report LA-UR-02-1839, Los Alamos National Laboratory, 2002.

[24] White, William. "Description of Silver Detector Setup", 13 Sept 2011. Personal E-mail.

[25] Wolfram Research, Inc. *Mathematica Edition: Version 9.0*. Champaign, IL, 2008.

[26] Wurden, et. al., G.A. "FRCHX Magnetized Target Fusion HEDLP Experiments". *LA-UR-08-0796*. submitted to IAEA 2008 Fusion Energy Conference, Geneva, Switzerland, Oct. 13-18, 2008. URL http://wsx.lanl.gov/Publications/IAEA08_synopsis-Wurden.pdf.

[27] Zhaohui, Song, Guan Xinyin, and Zhang Zichuan. "Silver Neutron Activaiton Detector for Measuring Bursts of 14 MeV Neutrons". Internet: http://isinn.jinr.ru/18/pdf/Song.pdf, Northwest Institute of Nuclear Texhnology. Xi'an, 710024, China [12 Feb 2012].

Vita

      Captain Melanie Mace was born in Davenport, Iowa and moved to Washington State when she was four. After graduating with honors at North Mason High School, she studied Engineering Physics at Embry-Riddle Aeronautical University (ERAU), Daytona Beach, Florida. She graduated with her Bachelor's Degree in Engineering Physics in May of 2005. Captain Mace commissioned into the United States Air Force in May of 2005 through the Reserve Officer Training Corps (ROTC) Detachment 157 at ERAU,. Following graduation and commissioning, she was assigned to Vandenberg AFB, CA where she went through Officer Space 100 and Intercontinental Ballistic Missile (ICBM) initial qualification training. She left Vandenberg AFB with a Highly Qualified end-of-course evaluation and went on the F.E. Warren AFB, WY. At F.E. Warren she continued to excel. After 4 years she had 9 Highly Qualified evaluations and ultimately left as the Chief of Training, Requirements Section Leader and an ICBM Combat Crew Instructor Commander. Following her assignment in ICBMs, she entered graduate school at the Air Force Institute of Technology (AFIT) in May of 2010 where she completed her Master's Degree in Nuclear Engineering. Her follow-on assignment is to Global Strike Command Headquarters where she will utilize her Master's degree to help solve operational problems.

REPORT DOCUMENTATION PAGE

1. REPORT DATE *(DD–MM–YYYY)*
14–06–2012

2. REPORT TYPE
Master's Thesis

3. DATES COVERED *(From — To)*
May 2010 — Jun 2012

4. TITLE AND SUBTITLE

Calibration of a Silver Detector using a PuBe source

5a. CONTRACT NUMBER

5b. GRANT NUMBER

5c. PROGRAM ELEMENT NUMBER

6. AUTHOR(S)

Melanie E. Mace, Captain, USAF

5d. PROJECT NUMBER
N/A

5e. TASK NUMBER

5f. WORK UNIT NUMBER

7. PERFORMING ORGANIZATION NAME(S) AND ADDRESS(ES)

Air Force Institute of Technology
Graduate School of Engineering Physics (AFIT/ENP)
2950 Hobson Way
WPAFB OH 45433-7765

8. PERFORMING ORGANIZATION REPORT NUMBER

AFIT/NUCL/ENP/12-J01

9. SPONSORING / MONITORING AGENCY NAME(S) AND ADDRESS(ES)

AFRL/RDHPP
Attn: Dr. William White
3550 Aberdeen Ave SE
Kirtland AFB, NM 87117-5776
505-853-4957, william.white@kirtland.af.mil

10. SPONSOR/MONITOR'S ACRONYM(S)

AFRL/RDHPP

11. SPONSOR/MONITOR'S REPORT NUMBER(S)

12. DISTRIBUTION / AVAILABILITY STATEMENT

DISTRIBUTION STATEMENT A: APPROVED FOR PUBLIC RELEASE; DISTRIBUTION UNLIMITED.

13. SUPPLEMENTARY NOTES

14. ABSTRACT

During the initial design of the Field Reversed Compression and Heating Experiment (FRCHX), magnetohydrodynamic simulations performed by Los Alamos National Laboratory using MACH2 predicted a neutron yield on the order of 10^{12} neutrons. However, Air Force Research Laboratory (AFRL) measurements indicate a total of 10^7-10^8 neutrons are generated from the FRCHX. A PuBe source was used to create a burst of neutrons to calibrate an AFRL silver detector based on distance to determine if the four order of magnitude discrepancy was cause by an improperly calibrated detector. It was determined that the calibration equation in use by AFRL for the silver detectors was correct within error at most points compared to this work. An alternate calibration equation $F_{PuBe} = 12.2D^2 + 3020D$ where D is the distance in inches from the source to the front face of the silver detector, was found using least squares techniques to reduce the residuals of the data collected using the PuBe source. The silver detectors were properly calibrated which does not account for the large order of magnitude difference observed between experiment and simulation of the FRCHX.

15. SUBJECT TERMS

Magnetized Target Fusion, silver detector, neutron activation analysis, PuBe source

16. SECURITY CLASSIFICATION OF:

a. REPORT	b. ABSTRACT	c. THIS PAGE
U	U	U

17. LIMITATION OF ABSTRACT
UU

18. NUMBER OF PAGES
99

19a. NAME OF RESPONSIBLE PERSON
Dr. John McClory

19b. TELEPHONE NUMBER *(include area code)*
(937) 255-3636, x3708; john.mcclory@afit.edu